



Buckling, Post-Buckling, Strength and Design of Angle Columns

P.B. Dinis¹, D. Camotim¹, N. Silvestre¹

Abstract

This paper presents procedures for the design of fixed-ended and pin-ended equal-leg angle columns with short-to-intermediate lengths. First, some numerical results concerning the buckling and post-buckling behavior of the angle columns are presented, (i) evidencing the main differences between the fixed-ended and pin-ended column responses, and (ii) showing the need for specific design procedures. Then, the paper reports an in-depth investigation aimed at gathering a large column ultimate strength data bank that includes (i) experimental values, collected from the literature, and (ii) numerical values, obtained from shell finite element analyses carried out in the code ABAQUS. The set of experimental results comprises 41 fixed-ended columns and 37 pin-ended columns, and the numerical results obtained concern 89 fixed-ended columns and 28 pin-ended columns – various cross-section dimensions, lengths and yield stresses are considered. Finally, the paper closes with the proposal of new design procedures, based on the Direct Strength Method (DSM), for fixed-ended and pin-ended angle columns. The two procedures adopt modified global and local strength curves, and it is shown that the proposed DSM approach leads to accurate ultimate strength estimates for short-to-intermediate columns covering a wide slenderness range.

1. Introduction

Thin-walled columns whose cross-sections have all wall mid-lines intersecting at a point (*e.g.*, angle, T-section and cruciform columns) are known to exhibit no primary warping – only secondary one. Thus, their torsional resistance is extremely low, which renders them highly susceptible to torsional or flexural-torsional buckling. Moreover, it is often hard to separate the torsional and local deformations and, thus, to distinguish between local and torsional buckling. Since these two instability phenomena are commonly associated with markedly different post-critical strength reserves, it is fair to say that this distinction may have far-reaching implications on the development of a rational model capable of providing accurate ultimate strength estimates for such columns.

The post-buckling behavior and strength of equal-leg angle columns has attracted the attention of several researchers in the past – *e.g.*, Wilhoite *et al.* (1984), Gaylord & Wilhoite (1985), Kitipornchai & Chan (1987), Popovic *et al.* (1999). Moreover, Young (2004), Ellobody & Young (2005) and Rasmussen (2005, 2006) performed recently experimental tests and shell finite element analyses on fixed-ended columns, aimed at obtaining ultimate loads and compare them with the predictions of the currently available design rules. Rasmussen and Young also put forward two approaches for the design of angle

¹ Department of Civil Engineering, ICIST, Instituto Superior Técnico, Technical University of Lisbon, Portugal.
<dinis@civil.ist.utl.pt>, <dcamotim@civil.ist.utl.pt> and <nunos@civil.ist.utl.pt>

columns, which are based on the Direct Strength Method (DSM – *e.g.*, Schafer 2008) global curve to estimate the flexural and local strengths. Chodraui *et al.* (2006) proposed a slightly different approach, differing from Rasmussen’s one in the fact that the column global strength is the lower of the flexural and torsional values, both obtained with the DSM global design curve. Following Chodraui’s work, (i) Maia (2008) and Maia *et al.* (2008) reported experimental tests on fixed-ended and pin-ended angle columns, and (ii) Mesacasa Jr. (2011) just performed a few further tests on fixed-ended angle columns. This last author also carried out a fairly complete compilation of the experimental results available in the literature, concerning both fixed-ended and pin-ended angle columns, explaining in some detail the main differences between the various test set-ups and procedures. Also very recently, Shifferaw & Schafer (2011) investigated the significant global post-buckling strength reserve observed in cold-formed steel angle column tests and provided some design guidance for locally slender cold-formed steel lipped and plain angles with fixed end supports. Finally, fresh numerical investigations, carried out by means of Generalized Beam Theory (GBT – *e.g.*, Camotim *et al.* 2010) and ABAQUS shell finite element analyses (SFEA) (Dinis *et al.* 2010a,b, 2011, 2012 and Dinis & Camotim 2011), (i) shed new light on how to distinguish between local and global buckling in equal-leg angle columns, and (ii) showed that (ii₁) both fixed-ended and pin-ended columns with short-to-intermediate lengths, buckling in flexural-torsional modes and having very similar critical stresses, exhibit different post-buckling behaviors and ultimate strengths (the amount of corner flexural displacements was found to play a key role in separating the various behaviors), and that (ii₂) the critical slenderness is inadequate to “measure” the ultimate strength of equal-leg angle columns.

This work reports the numerical and experimental results obtained with the aim of developing a rational DSM-based design approach for short-to-intermediate equal-leg angle columns – both fixed-ended and pin-ended (but with the end section secondary warping prevented) columns are considered. After showing some illustrative numerical results concerning the buckling and post-buckling behavior of such columns (Dinis *et al.* 2010a, 2011, 2012, Dinis & Camotim 2011), the paper addresses the assembly of column ultimate strength data, intended to provide the basis for the development, calibration and validation of specific design procedures for equal-leg angle columns. It consists of (i) collecting and organizing experimental values available in the literature and (ii) determining numerical (SFEA) values by performing a fairly extensive parametric study. The output of this effort are 76 experimental and 117 numerical ultimate load values concerning columns with either pinned or fixed end supports and various cross-section dimensions, lengths and yield stresses (Silvestre *et al.* 2012). Finally, the column ultimate load “data bank” gathered is used to propose and assess the efficiency (accuracy and economy) of a DSM approach to predict the ultimate strength of the angle columns under consideration – it involves distinct procedures for fixed-ended and pin-ended columns.

2. Buckling and Post-Buckling Behavior

One presents and discusses here the main results of a recent investigation on the buckling and post-buckling behavior and ultimate strength of thin-walled steel ($E=210GP$ and $\nu=0.3$) angle columns (Dinis *et al.* 2010a, 2011, 2012, Dinis & Camotim 2011). The columns analyzed exhibit (i) pinned (but with the secondary warping prevented) and fixed end sections, (ii) equal legs ($70\times 70\text{ mm}$ and $t=1.2\text{ mm}$ – the effect of rounded corners is disregarded) and (iii) short-to-intermediate lengths. Almost all the numerical results were obtained through ABAQUS (Simulia 2008) shell finite element analyses, (i) adopting column discretizations into fine 4-node isoparametric element meshes (length-to-width ratio close to 1) and (ii) modeling the column supports by (ii₁) fully attaching the member end sections to *rigid end-plates* (thus ensuring the secondary warping and *local* displacement/rotation restraints) and (ii₂) preventing both the

major and minor-axis flexural rotations (fixed supports – F condition) or only the major-axis flexural rotations (pinned cylindrical hinge supports – P condition²) – the torsional rotations are prevented in both cases. However, in order to characterize and distinguish between local and global buckling of angle columns, GBT analyses are also performed using GBTUL (Bebiano *et al.* 2008a,b).

2.1 Buckling Behavior

The curves shown in Fig. 1(a) provide the variation of P_{cr} (critical load, obtained from ABAQUS shell finite element analysis) with the length L (logarithmic scale), both for fixed-ended (F curve) and pin-ended (P curve) columns. This figure also depicts single half-wave buckling loads, $P_{b,1}$, yielded by GBT analyses including 7 deformation modes: 4 global (1-4) and 3 local (5-7). As for Fig. 1(b), it displays the GBT modal participation diagrams for the columns with both end support conditions – they provide the contributions of each GBT deformation mode to the column single half-wave buckling modes (Dinis *et al.* 2010a). Finally, Fig. 1(c) shows the buckling mode shapes of the pin-ended columns with $L=100, 364, 1000\text{ cm}$, as well as the in-plane shapes of the first 6 deformation modes (axial extension excluded). These buckling results prompt the following remarks:

- (i) For the entire length range, the critical buckling modes of all columns involve only deformation modes **2, 3, 4** and **6**.
- (ii) Due to the cross-section symmetry with respect to the major-axis, all the short-to-intermediate columns buckle in flexural-torsional modes, combining participations from deformation modes **4** (torsion) and **2** (major-axis flexure), which correspond to fairly uniform critical loads defining almost horizontal “plateaus” in the P_{cr} vs. L curves. The participations of modes **2** and **4** continuously vary with the column length – the former is imperceptible for the shorter columns and only becomes visible as L increases (the growth occurs at a fairly small pace).
- (iii) Both the pin-ended and fixed-ended columns display similar buckling features: (iii₁) P_{cr} decreases monotonically with L and corresponds to single half-wave buckling, (iii₂) the GBT and ABAQUS

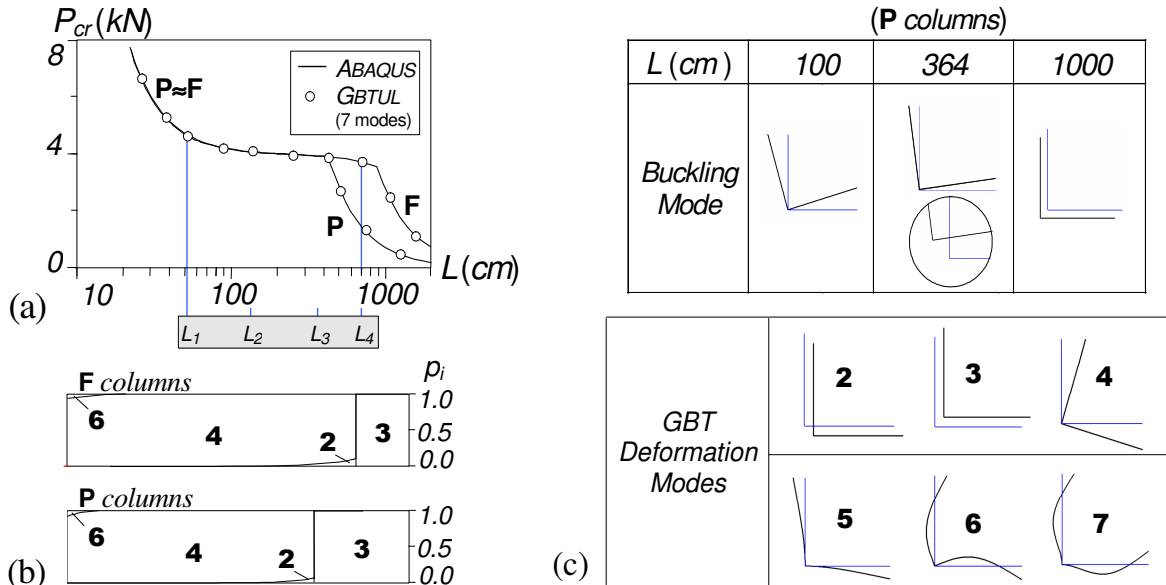


Figure 1: (a) P_{cr} vs. L curves and (b) GBT modal participation diagrams (F and P columns), and (c) in-plane shapes of 3 buckling modes and first 5 GBT deformation modes (P columns)

² These are the end support conditions adopted in the “pin-ended angle column experimental tests” reported in the literature.

results virtually coincide, and (iii₃) the torsion mode **4** plays a key role, as it participates in the critical buckling modes of all but the long columns, which exhibit pure minor-axis flexural buckling modes (only mode **3**).

- (iv) Compared to the short-to-intermediate F columns, the P columns only differ in the smaller length range corresponding to the end of the “plateau”, due to the 75% drop of the minor-axis flexural buckling loads – the transition from flexural-torsional buckling to flexural buckling occurs for $L=420\text{cm}$ (P columns) and $L=890\text{cm}$ (F columns). For columns shorter than $L=420\text{cm}$ (P column transition length), the local and flexural-torsional buckling loads and mode shapes of the F and P columns with the same length are exactly the same.
- (v) The post-buckling results presented in the next subsection concern short-to-intermediate angle columns with the following length values (see Fig. 1(a)): $L_1=53\text{cm}$, $L_2=133\text{cm}$, $L_3=364\text{cm}$ and $L_4=700\text{cm}$ – 4 fixed-ended columns (F_1-F_4 – $22.1 \leq f_{cr} \leq 27.5 \text{ N/mm}^2$) and 3 pin-ended columns (P_1-P_3 – $23.4 \leq f_{cr} \leq 27.5 \text{ N/mm}^2$).

2.2 Elastic and Elastic-Plastic Post-Buckling Behavior

ABAQUS shell finite element analyses are employed to investigate the elastic and elastic-plastic post-buckling behavior of fixed-ended and pin-ended angle columns (i) exhibiting the lengths indicated before, (ii) containing critical-mode initial imperfections with amplitude equal to 10% of the wall thickness t (flexural-torsional shapes with mid-span torsional rotations equal to about $\beta_0=0.1^\circ$ for the angle section $70 \times 70 \times 1.2\text{mm}$) and (iii) exhibiting various yield-to-critical stress ratios (Dinis *et al.* 2010b, 2012, Dinis & Camotim 2011).

Figures 2(a)-(c) show the upper parts ($P/P_{cr} > 0.6$) of the F_1-F_4 column post-buckling equilibrium paths (i) P/P_{cr} vs. β , P/P_{cr} vs. d_M/t and P/P_{cr} vs. $d_m/t - \beta$, d_M and d_m are the mid-span web chord rigid-body rotation and corner displacements caused by major and minor-axis flexure, respectively. As for Figs. 3(a)-(b), they concern the F_2-F_4 columns and provide the longitudinal profiles of the two corner displacements at four equilibrium states (increasing P/P_{cr} values) – note that (i) the horizontal coordinate is normalized to the column length (x_3/L) and (ii) the d_M/t and d_m/t scales are significantly different for the three columns (*e.g.*, the F_4 column values are 80 times larger than their F_2 column counterparts). The observation of these elastic post-buckling results prompts the following comments:

- (i) All column post-buckling behaviors involve the simultaneous occurrence of cross-section torsional rotations and flexural (corner) displacements. The relative importance of the latter has strong impact on the column post-buckling response, namely on its post-critical strength reserve.

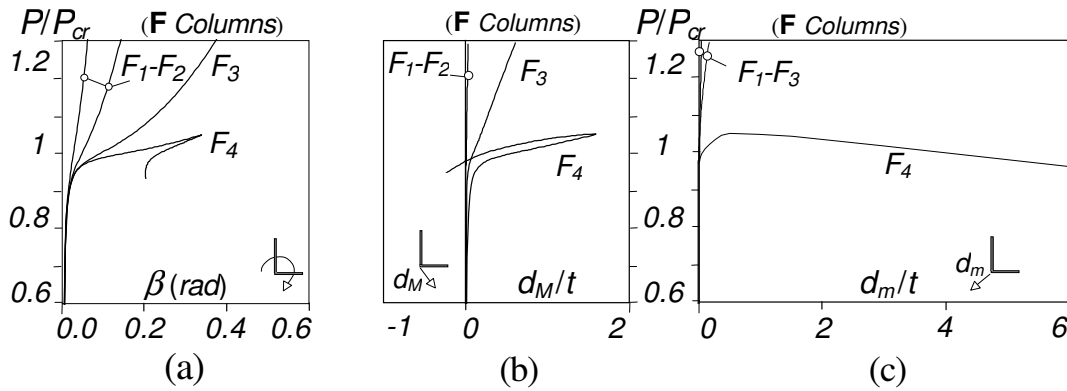


Figure 2: F_1-F_4 columns: (a) P/P_{cr} vs. β , (b) P/P_{cr} vs. d_M/t and (c) P/P_{cr} vs. d_m/t equilibrium paths

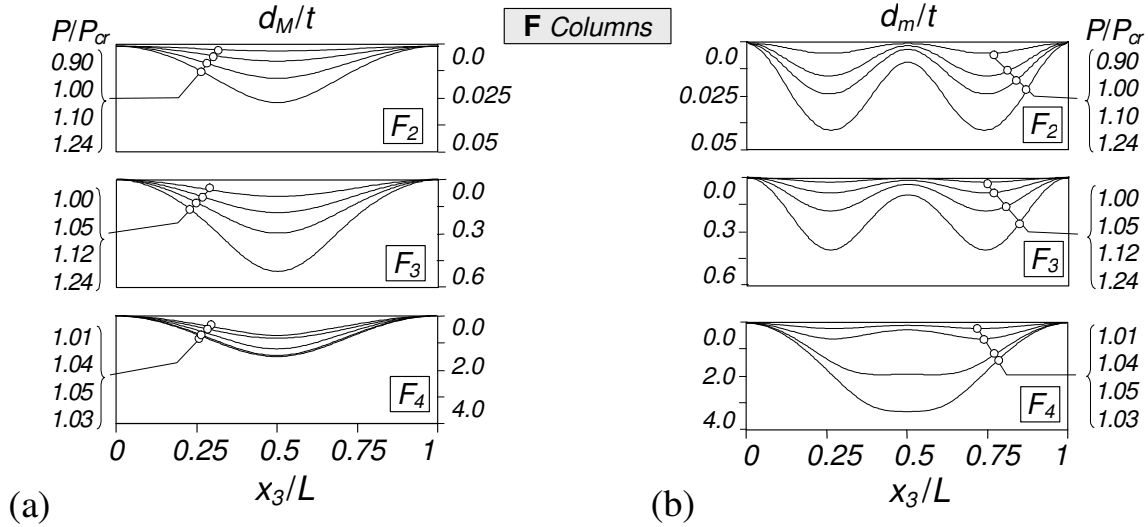


Figure 3: F_2 - F_4 columns: (a) d_M/t and (b) d_m/t longitudinal profiles

- (ii) Indeed, two column “families” can be identified, according to their post-buckling behavior:
 - (ii₁) the shorter F_1 - F_3 columns ones (the F_1 and F_2 columns have virtually identical equilibrium paths), which are clearly stable (fairly high post-critical strengths) and exhibit very small corner displacements, and
 - (ii₂) the longer F_4 column, which exhibits significant corner displacements and has a limit point, followed by a significant torsional rotation reversal (see Fig. 2(a)). This torsional rotation reversal is due to an abrupt switch from a single half-wave to three half-waves soon after the peak load is reached (Dinis & Camotim 2011, Dinis *et al.* 2012).
- (iii) Since major-axis flexure participates in the column critical buckling modes (see the participation of deformation mode 2 in Fig. 1(b)) and, thus, integrates the corresponding initial geometrical imperfections, it is not surprising that (iii₁) d_M values progressively grow with the applied load and that (iii₂) their longitudinal profiles exhibit the typical fixed-ended column critical buckling mode shape: one inner half-wave and two outer “quarter-waves” (to ensure null end slopes).
- (iv) The emergence of minor-axis flexure (d_m displacements), which does not participate in the column critical buckling modes and exhibits longitudinal profiles with three inner half-waves (and two outer “quarter-waves” to ensure null end slopes), stems from the longitudinal variation of the torsional rotations. These rotations cause non-linear cross-section mid-line longitudinal stress distributions that vary along the column axis according to a “three half-wave” pattern, which lead to effective centroid shifts (towards the cross-section corner) following that same longitudinal pattern (Stowell 1951, Dinis & Camotim 2011, Dinis *et al.* 2012). These effective centroid shifts are responsible for the (positive) minor-axis flexural displacements that have some impact on the fixed-ended angle column response. In the longer (F_4) column, this impact is overshadowed by the occurrence of fairly strong interaction with flexural buckling. Indeed, for this column length, the flexural-torsional and flexural buckling loads are fairly close and become much closer due to the axial stiffness reduction associated with the flexural-torsional (“local”) post-buckling behavior.
- (v) Due to the relevance of the corner displacements (mostly the minor-axis flexural ones), the behavior of fixed-ended equal-leg angle columns can not be viewed as the “sum” of two fixed-ended (longitudinally) pinned-free (transversally) long plates, unlike one would be tempted to anticipate. In particular, the cross-section longitudinal normal stress distributions develop to be far from parabolic as post-buckling progresses. Recently, the authors (Dinis *et al.* 2010b, 2012) have shown that

preventing the corner displacements makes it possible to recover the pinned-free long plate post-buckling behaviour. In the case of the (long) F_4 column, the post-buckling behavior is significantly altered – it changes to clearly stable (no limit point) and the normal stress distributions (not shown here) change drastically, becoming parabolic with the higher value at the pinned edge (*i.e.*, in line with the general belief).

Next, one investigates how releasing the end sections minor-axis flexural rotations affects the post-buckling behavior of angle columns with short-to-intermediate lengths. Figures 4(a)-(c) show the upper parts of the P_1 - P_3 column post-buckling equilibrium paths P/P_{cr} vs. β , P/P_{cr} vs. d_M/t and P/P_{cr} vs. d_m/t , while Figs. 5(a)-(b) display the P_2 - P_3 column d_M/t and d_m/t longitudinal profiles at three equilibrium states (increasing P/P_{cr} values). The observation of these pin-ended column post-buckling results, as well as the comparison with their fixed-ended counterparts, leads to the following conclusions:

- (i) There are again two pin-ended column “families”, concerning their post-buckling behavior: (i₁) the P_1 column is clearly stable and exhibits minute mid-span corner displacements, and (i₂) the P_2 - P_3 columns are barely stable, experience significant mid-span corner displacements and exhibit limit points – either abrupt and followed by torsional rotation reversal (P_2 column) or smooth and without torsional rotation reversal (P_3 column) – the amount of corner flexural displacements plays a key role in separating the various post-buckling behaviors.
- (ii) The fixed-ended and pin-ended column equilibrium paths share a few columns common features: (ii₁) the d_M displacements remain always very small (they grow with L and their longitudinal profiles retain the typical fixed-ended critical buckling mode shape) and (ii₂) the rotation reversals coincide with the torsional rotation “switch” from a single to three half-waves.
- (iii) However, there are some important differences between the evolutions of the d_m/t longitudinal profiles in the fixed-ended and pin-ended columns: while the former exhibit three inner half-waves (plus two external “quarter-waves” to ensure null end slopes), the latter apparently exhibit just one half-wave³. Moreover, note that the pinned column d_m values are significantly higher (about ten times) than their d_M counterparts – their magnitude are similar (and small) for fixed-ended (before the interaction with the minor-axis flexural buckling mode, of course).

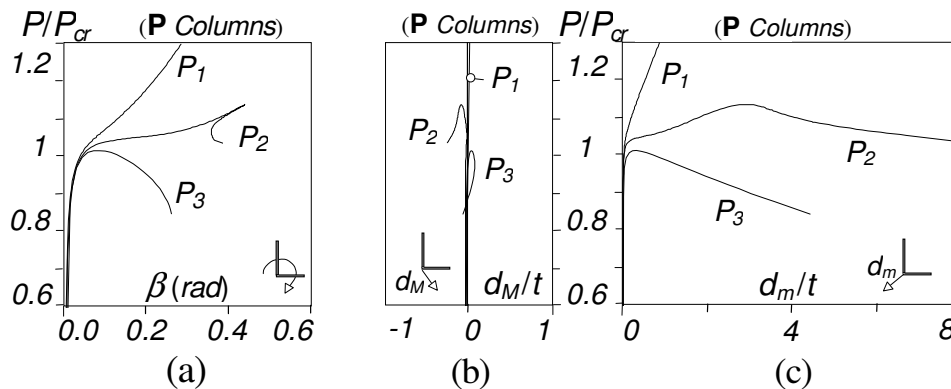


Figure 4: P_1 - P_3 columns: (a) P/P_{cr} vs. β , (b) P/P_{cr} vs. d_M/t and (c) P/P_{cr} vs. d_m/t equilibrium paths

³ A closer look at the d_m/t longitudinal profiles of the P_2 and P_3 columns reveals that the former exhibits a half-wave with a “flat” central region that decreases as the loading progresses – this does not occur in the P_3 column, which exhibits a “well curved” half-wave. This “flat” central region corresponds to the combination of (i) a dominant “well curved” half-wave with (ii) less relevant three half-waves – the presence of the latter is virtually imperceptible in the P_3 column (Dinis *et al.* 2012).

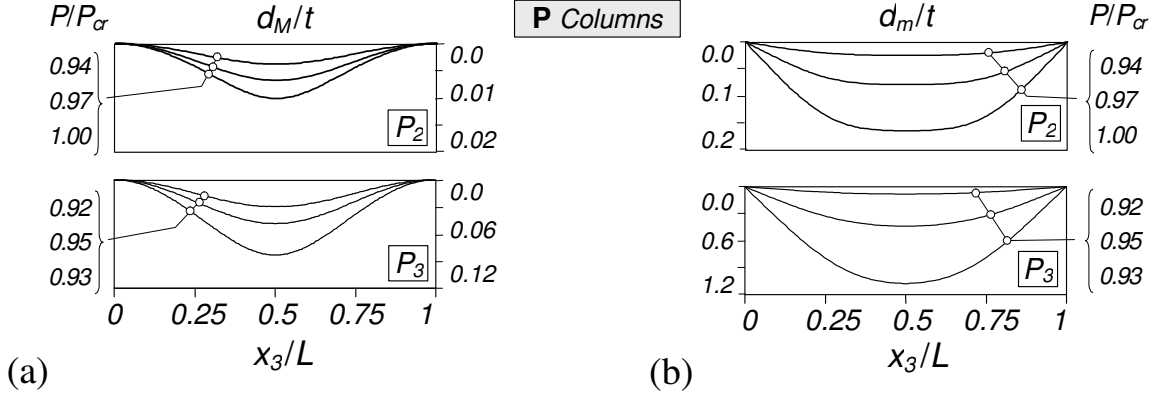


Figure 5: P_2 - P_3 columns: (a) d_M/t and (b) d_m/t longitudinal profiles

- (iv) The differences described in the previous item stem from the absence of the minor-axis end moments, which means that it is no longer possible to oppose the minor-axis bending caused by the “effective centroid shifts” occurring due to the cross-section normal stress redistribution (*e.g.*, Young & Rasmussen 1999). Indeed, although the mechanical reasoning behind the development of the three half-wave d_m profile remains valid for the pin-ended columns (recall that the end section secondary warping and torsional rotation are still prevented), the predominance of the “well curved” (sinusoidal) half-wave component now largely overshadows it. Such predominance is even clearer in the longer columns, such as the P_3 one, due to the more intense interaction with minor-axis flexural buckling (closer flexural-torsional and flexural buckling loads).

The elastic-plastic behavior and strength of fixed-ended and pin-ended short-to-intermediate angle columns is briefly addressed now. The results presented concern columns (i) still containing critical-mode initial imperfections with $0.1t$ amplitude, and (ii) exhibiting four yield-to-critical stress ratios ($f_y/f_{cr} \approx 1.3, 2.5, 5.0 - f_y = 30, 60, 120 \text{ N/mm}^2$ and “average” $f_{cr} = 24 \text{ N/mm}^2$)⁴ – note that, for comparative purposes, some elastic results presented earlier are shown again (they correspond to $f_y/f_{cr} = \infty$).

Figure 6(a) depicts typical shorter fixed-ended column elastic-plastic equilibrium paths. It shows the upper portions ($P/P_{cr} > 0.5$) of the F_3 column P/P_{cr} vs. β paths concerning the yield-to-critical stress ratios $f_y/f_{cr} \approx 1.3, 2.5, 5.0$ (and also the elastic path already shown in Fig. 2(a)). Figure 6(b), on the other hand, displays three plastic strain diagrams, corresponding to equilibrium states located along the $f_y/f_{cr} \approx 2.5$ equilibrium path (as indicated in Fig. 6(a)) and including the column collapse mechanism. As for Figs. 7(a)-(b), they illustrate a typical longer fixed-ended column elastic-plastic post-buckling behavior. They show the upper portions of the F_4 column P/P_{cr} vs. β paths concerning four f_y/f_{cr} values and also the column deformed configuration and plastic strain evolution, for $f_y/f_{cr} \approx 2.5$. After the observation of all these results, the following remarks are appropriate:

- (i) While the F_3 columns with $f_y/f_{cr} \approx 1.3, 2.5$ fail at the onset of yielding, their $f_y/f_{cr} \approx 5.0$ counterpart exhibits a very small elastic-plastic strength reserve.
- (ii) The F_3 column ultimate load grows noticeably with f_y – *e.g.*, an increase from 30 to 120 N/mm^2 more than doubles the load-carrying capacity.
- (iii) Diagram *I* in Fig. 6(b) shows that, in the F_3 columns, yielding starts around the quarter and three quarter-span zones of the corner longitudinal edge, where the shear and longitudinal normal stresses, due to the torsional rotation variation, are higher (Stowell 1951 and Dinis *et al.* 2012).

⁴ Note that, in order to cover a wide slenderness range, some unrealistically low yield stresses were considered.

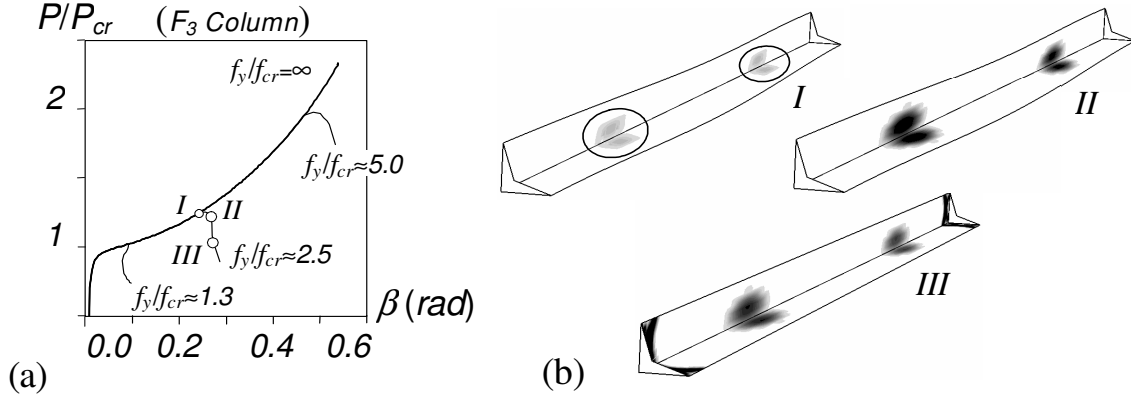


Figure 6: F_3 column elastic-plastic post-buckling behavior: (a) P/P_{cr} vs. β equilibrium paths, for $f_y/f_{cr} \approx 1.3, 2.5, 5.0$, and (b) plastic strain diagrams and failure mechanism, for $f_y/f_{cr} \approx 2.5$

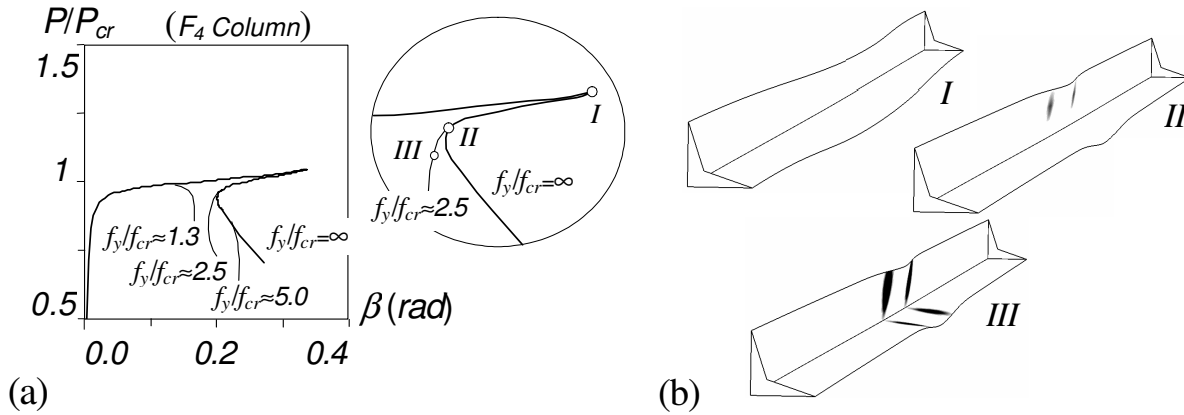


Figure 7: F_4 column elastic-plastic post-buckling behavior: (a) P/P_{cr} vs. β equilibrium paths, for $f_y/f_{cr} \approx 1.3, 2.5, 5.0$, and (b) plastic strain diagrams and (elastic) failure mode, for $f_y/f_{cr} \approx 2.5$

(iv) On the other hand, the longer F_4 column ultimate strength is practically insensitive to f_y , since the collapse is predominantly caused by geometrically non-linear effects. Indeed, for $f_y/f_{cr} \approx 2.5, 5.0$ the column remains elastic up until failure, as the onset of yielding only takes place well inside the equilibrium path descending branch – it occurs in the middle of the vertical leg mid-span region, as illustrated in Fig. 7(b) (diagram II).

A similar investigation was carried out for pin-ended columns. Figures 8(a)-(b) display (i) the upper parts ($P/P_{cr} > 0.5$) of the P/P_{cr} vs. β paths concerning P_2 columns with $f_y/f_{cr} \approx 1.3, 2.5, 5.0, \infty$, and (ii) the plastic strain evolution and collapse mechanism of the P_2 column with $f_y/f_{cr} \approx 2.5$. The observation of these post-buckling results prompts the following comments:

- (i) There is virtually no elastic-plastic strength reserve or ductility prior to failure – yielding starts in the middle of the vertical leg quarter-span and three quarter-span (see diagram I in Fig. 8(b)) and precipitates the column collapse.
- (ii) There is a rather small variation of the column ultimate load with the yield stress – e.g., a rise from 30 to 120 N/mm^2 entails a small load-carrying capacity increase (only 9.4%). Moreover, there is no benefit in increasing the yield stress beyond five times f_{cr} , since for $f_y/f_{cr} \approx 5.0$ the collapse occurs abruptly in the elastic range (the $f_y/f_{cr} \approx 5.0$ and $f_y/f_{cr} \approx \infty$ curves share the same limit point).

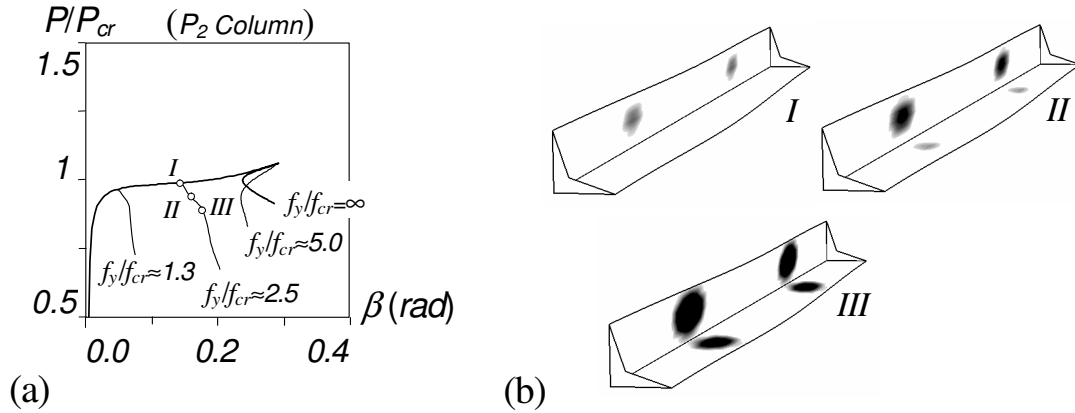


Figure 8: P_2 column elastic-plastic post-buckling behavior: (a) P/P_{cr} vs. β equilibrium paths, for $f_y/f_{cr} \approx 1.3, 2.5, 5.0$, and (b) plastic strain diagrams and failure mode, for $f_y/f_{cr} \approx 2.5$

- (iii) The above P_2 column post-buckling behavior features are also exhibited, to an even larger extent, by the longer pin-ended columns, such as the P_3 one – recall its elastic post-buckling equilibrium paths, shown in Figs. 4(a)-(c), which display smooth limit points for $P/P_{cr} \approx 1.0$.

The markedly different elastic and elastic-plastic post-buckling behaviors displayed by the fixed-ended and pin-ended short-to-intermediate equal-leg angle columns implies that there is a significant discrepancy between their ultimate strengths P_u associated with a given yield stress. Since all those columns have virtually identical critical stresses (thus sharing a common critical slenderness $\lambda = (P_y/P_{cr})^{0.5}$), their P_u/P_y values may exhibit a high “vertical dispersion” with respect to λ – this behavioral feature must be adequately accounted for by an efficient design procedure for equal-leg angle columns.

3. Ultimate Strength Data: Test Results and Numerical Predictions

Following the findings reported by Dinis *et al.* (2010b, 2011, 2012) and Dinis & Camotim (2011), which were summarized above, it was decided to assess the performance of the existing design rules for cold-formed steel equal-leg angle columns. The first step towards achieving this goal consists of putting together a fairly large column ultimate strength data bank, comprising (i) experimental test results performed by other researchers, collected from the available literature, and (ii) numerical results, obtained by means of the shell finite element model developed earlier.

The experimental results gathered concern (i) 41 fixed-ended columns, tested by Popovic *et al.* (1999), Young (2004) and Mesacasa Jr. (2011)⁵, and (ii) 37 pin-ended columns (with cylindrical supports), tested by Wilhoite *et al.* (1984), Popovic *et al.* (1999), Chodraui *et al.* (2006) and Maia *et al.* (2008). The fixed-ended columns had nominal cross-section dimensions (i) $50 \times 2.5 \text{ mm}$, $50 \times 4.0 \text{ mm}$ and $50 \times 5.0 \text{ mm}$ (Popovic *et al.* 1999), (ii) $70 \times 1.2 \text{ mm}$, $70 \times 1.5 \text{ mm}$ and $70 \times 1.9 \text{ mm}$ (Young 2004) and (iii) $60 \times 2.0 \text{ mm}$ (Mesacasa Jr. 2011). The nominal cross-section dimensions of the pin-ended columns were (i) $70 \times 3.0 \text{ mm}$ (Wilhoite *et al.* 1984), (ii) $50 \times 2.5 \text{ mm}$, $50 \times 4.0 \text{ mm}$ and $50 \times 5.0 \text{ mm}$ (Popovic *et al.* 1999), and (iii) $60 \times 2.4 \text{ mm}$ (Chodraui *et al.* 2006 and Maia 2008). Further details concerning the measured specimen dimensions and steel properties can be found in the publications mentioned above and included in the paper reference list.

⁵ Four fixed-ended columns tested by Maia *et al.* (2008) were excluded from this study, since the ultimate strengths reported seem excessively low when compared with the numerical results obtained by the same authors, adopting fair-to-high torsional initial imperfections ($0.64t$ and $1.55t$). In the authors’ opinion, these fixed-ended columns contain abnormally large initial imperfections and/or load eccentricities (maybe caused by the procedure adopted to ensure the column end section fixity).

For each cross-section geometry, specimen length L and measured yield stress f_y , Tables 1 (fixed-ended columns) and 2 (pin-ended columns) provides the test results, namely the column ultimate stress f_u . Concerning the information given in Table 2 (pin-ended columns), it should be mentioned that the 9 pin-ended columns tested by Wilhoite *et al.* (1984) had only three different lengths (823, 1227, 1636 mm), since three specimens with (approximately) the same length were tested. The repeated test results were included herein because they show the following peculiar feature: while (i) the three shorter columns ($L=823$ mm) provided similar ultimate strengths, (ii) those concerning the intermediate columns ($L=1227$ mm) showed some scatter (higher and lower ultimate strength values 11.5% apart) and (iii) the longer columns ($L=1636$ mm) showed even more scatter (22.5% difference). In the tests by Wilhoite *et al.* (1984), a small clearance was built into the pin-ended bearings to avoid locking, and a load eccentricity may have been induced by this clearance. Since the bearings were manufactured to a tolerance that ensured that the load eccentricity induced would not exceed $1/1000$ of the longer column length, it may have happened that non-negligible load eccentricities prevailed in the tests and influenced the ultimate strength. Moreover, the 50×2.5 mm pin-ended columns tested by Popovic *et al.* (1999) were not concentrically loaded, as they were reported to exhibit load eccentricities of roughly $\pm L/1000$ along the major-axis ($+L/1000$ and $-L/1000$ eccentricities increase compression at the leg tips and corner, respectively). They are, in fact, beam-columns with similar lengths that exhibit different ultimate strengths f_u because of the eccentricity sign (the lower f_u values correspond to $+L/1000$ eccentricities). It is also possible to conclude that the percentage difference between the $+L/1000$ and $-L/1000$ eccentricity results also grows with L . Since the load eccentricity may be viewed as a geometrical imperfection (both affect similarly the column response), these results further indicate that the pin-ended columns are also sensitive to the minor-axis initial imperfection sign.

The numerical (SFEA) results obtained concern (i) 89 fixed-ended columns, displaying the cross-section dimensions 70×1.2 mm, 50×1.2 mm and 50×2.6 mm, and (ii) 28 pin-ended columns, all with the cross-section 70×1.2 mm. The column lengths were selected to ensure that critical buckling occurs in flexural-torsional modes (*i.e.*, they fall within the P_{cr} vs. L curve “horizontal plateaus” – see Fig. 1(a)). Their values are (i) 532, 980, 1330, 1820, 2520, 3640, 4200, 5320, 7000, 8900 mm (fixed-ended 70×1.2 mm columns), (ii) 1500, 2000, 2500, 3000, 4000 mm (fixed-ended 50×1.2 mm columns), (iii) 1000, 1500, 2000 mm (fixed-ended 50×2.6 mm columns), and (iv) 532, 980, 1330, 1820, 2520, 3640, 4200 mm (pin-ended 70×1.2 mm columns). In all the analyses, the steel material behavior is modeled as elastic-perfectly plastic ($E=210$ GPa, $\nu=0.3$) and both the residual stresses and rounded corner effects are disregarded. Preliminary numerical studies showed that the combined influence of strain hardening, residual stresses and rounded corner effects has little impact on the angle column ultimate strength (all differences below 3%), which is in line with the findings reported by other authors, namely Ellobody & Young (2005) and Shi *et al.* (2009). As mentioned earlier, the yield stresses f_y were selected to cover a wide critical slenderness range, thus leading to the consideration of a few unrealistic (small) values. They are (i) 30, 60, 120, 235, 400, 500 N/mm² (fixed-ended 70×1.2 mm columns), (ii) 120, 235, 400, 500 N/mm² (fixed-ended 50×1.2 mm columns), (iii) 120, 235, 400 N/mm² (fixed-ended 50×2.6 mm columns) and (iv) 30, 60, 120, 235 N/mm² (pin-ended 70×1.2 mm columns).

Following the behavior observed in the experimentally tested columns (described before), namely the length-dependency of the imperfection-sensitivity, a preliminary study was carried out to identify the most detrimental imperfection shape – critical flexural-torsional shape and/or minor axis flexural shape. For column lengths corresponding to the left and intermediate parts of the $P_{cr}(L)$ curve horizontal plateaus, the flexural-torsional imperfections were found to be the most detrimental ones (the columns are virtually insensitive to the minor-axis flexural imperfections). In these (short-to-intermediate) columns,

Table 1: Fixed-ended column experimental ultimate stresses and their estimates according to (i) the design method developed by Young (2004) and (ii) the proposed DSM-based approach

Section	L (mm)	Buckling analysis			Test f_u (N/mm ²)	Young (2004) f_u/f_p	DSM-F f_{nle} (N/mm ²)	Test-to- Predicted f_u/f_{nle}
		f_{cr1} (N/mm ²)	f_{cre} (N/mm ²)	f_y (N/mm ²)				
Popovic <i>et al.</i> (1999) 50x2.5	150	376	38074	396	308	1.30	329	0.94
	550	198	2832	396	225	1.01	250	0.90
	970	186	910	396	173	0.90	214	0.81
	1379	180	450	396	154	1.00	172	0.89
	1747	174	281	396	130	1.11	133	0.98
	2199	167	177	396	110	1.44	89	1.24
	2598	159	127	396	93	1.70	63	1.46
Popovic <i>et al.</i> (1999) 50x4.0	150	961	38826	388	424	1.26	385	1.10
	970	460	928	388	314	1.19	286	1.10
	1381	430	458	388	250	1.33	216	1.16
	1743	398	288	388	178	1.41	152	1.17
Popovic <i>et al.</i> (1999) 50x5.0	150	1431	37819	388	414	1.15	385	1.07
	970	667	904	388	307	1.20	288	1.06
	1378	602	448	388	216	1.21	213	1.02
	1749	531	278	388	180	1.56	148	1.22
Young (2004) 70x1.2	250	37.6	28143	550	143	1.16	177	0.81
	1000	22.3	1759	550	113	1.03	128	0.88
	1500	21.7	782	550	92	0.99	107	0.86
	2000	21.4	440	550	76	1.04	84	0.90
	2500	21.3	281	550	70	1.28	62	1.13
	3000	21.2	195	550	48	1.10	49	0.99
	3500	21.1	144	550	35	0.96	40	0.87
Young (2004) 70x1.5	250	61.8	27852	530	189	1.26	208	0.90
	1000	36.6	1741	530	148	1.12	151	0.98
	1500	35.6	774	530	120	1.07	127	0.94
	2000	35.2	435	530	83	0.93	100	0.83
	2500	34.9	279	530	75	1.13	74	1.01
	3000	35.6	193	530	62	1.17	58	1.07
	3500	34.4	142	530	55	1.24	47	1.16
Young (2004) 70x1.9	250	96.7	28379	500	212	1.22	237	0.90
	1000	57.0	1774	500	180	1.15	174	1.03
	1500	55.4	788	500	134	1.00	147	0.91
	2000	54.6	443	500	102	0.94	118	0.86
	2500	54.0	284	500	84	1.03	89	0.95
	3000	53.4	197	500	56	0.87	68	0.82
	3500	52.8	145	500	54	1.03	55	0.98
Mesacasa Jr. (2011) 60x2.0	400	103	7411	350	177	–	191	0.93
	600	93	3294	350	166	–	179	0.93
	900	89	1464	350	137	–	166	0.83
	1200	87	823	350	128	–	152	0.85
	1800	84	366	350	88	–	118	0.74
					Mean	1.15	Mean	0.98
					Sd. Dev.	0.18	Sd. Dev.	0.14

Table 2: Pin-ended column experimental ultimate stresses and their estimates according to (i) the design method developed by Rasmussen (2006) and (ii) the two proposed DSM-based approaches

Section	L (mm)	Buckling analysis			Test f_u (N/mm ²)	Rasmussen (2006) f_u/f_p	DSM-F f_{nle} (N/mm ²)	Test-to- Predicted f_u/f_{nle}	DSM-P f_{nle} (N/mm ²)	Test-to- Predicted f_u/f_{nle}
		f_{cr1} (N/mm ²)	f_{cre} (N/mm ²)	f_y (N/mm ²)						
Wilhoite <i>et al.</i> (1984) 70x3.0	823	155	596	465	174	1.18	191	0.91	133	1.31
	823	155	596	465	174	1.18	191	0.91	133	1.31
	1227	149	268	465	140	1.27	121	1.16	109	1.28
	1227	149	268	465	144	1.30	121	1.19	109	1.32
	1227	149	268	465	156	1.41	121	1.29	109	1.43
	1636	145	151	465	116	1.48	75	1.54	75	1.54
	1636	145	151	465	125	1.59	75	1.66	75	1.66
	1636	145	151	465	142	1.81	75	1.89	75	1.89
Popovic <i>et al.</i> (1999) 50x2.5	286	237	2618	396	187	1.06	264	0.71	198	0.95
	285	237	2637	396	212	1.07	264	0.80	198	1.07
	490	202	892	396	158	1.07	219	0.72	167	0.95
	490	202	892	396	180	1.03	219	0.82	167	1.08
	674	192	471	396	139	1.13	180	0.77	151	0.92
	675	192	470	396	213	1.42	179	1.19	150	1.42
	900	187	264	396	113	1.19	131	0.86	125	0.90
	900	187	264	396	144	1.21	131	1.10	125	1.16
	1099	184	177	396	79	1.06	89	0.90	89	0.90
	1100	184	177	396	111	1.14	88	1.25	88	1.25
Popovic <i>et al.</i> (1999) 50x4.0	285	605	2689	388	367	–	351	1.05	344	1.07
	490	512	910	388	295	–	289	1.02	285	1.04
	675	484	479	388	205	–	221	0.93	221	0.93
Popovic <i>et al.</i> (1999) 50x5.0	285	900	2619	388	360	–	350	1.03	350	1.03
	490	758	886	388	277	–	286	0.97	286	0.97
	490	758	886	388	273	–	286	0.95	286	0.95
	675	714	467	388	214	–	218	0.98	218	0.98
	675	714	467	388	196	–	218	0.90	218	0.90
Chodraui <i>et al.</i> (2006) 60x2.4	480	143	1307	371	112	–	200	0.56	126	0.89
	835	130	432	371	105	–	149	0.70	109	0.96
	1195	126	211	371	83	–	98	0.85	90	0.92
	1550	124	125	371	76	–	63	1.21	63	1.21
Maia <i>et al.</i> (2008) 60x2.4	480	144	1320	357	112	–	197	0.57	127	0.88
	650	136	720	357	130	–	174	0.75	117	1.11
	835	131	436	357	105	–	149	0.70	110	0.95
	1000	129	304	357	144	–	126	1.14	103	1.40
	1195	127	213	357	81	–	99	0.82	91	0.89
	1350	126	167	357	103	–	81	1.27	78	1.31
	1550	126	127	357	76	–	63	1.20	63	1.20
					Mean	1.26	Mean	1.01	Mean	1.13
					Sd. Dev.	0.21	Sd. Dev.	0.29	Sd. Dev.	0.25

flexural-torsional imperfections with amplitude equal to 10% of the wall thickness t were adopted. Conversely, for column lengths associated with the right part of the $P_{cr}(L)$ curve horizontal plateaus, the minor-axis flexural imperfections were shown to be much more relevant than their “critical” flexural-

torsional counterparts. In these (intermediate-to-long) columns, the adopted initial imperfections combine (i) a “critical” flexural-torsional component, of amplitude equal to 10% of the wall thickness t , and (ii) a “non-critical” minor-axis flexural component, of amplitude equal to $L/750$ (fixed-ended columns) or $L/1000$ (pin-ended columns) – these amplitudes are in line with the means of the values measured in the specimens tested by Popovic *et al.* (1999) and Young (2004), respectively.

The combined “flexural-torsional + minor-axis flexural” initial imperfections were considered for the lengths (i) 4200, 5320, 7000, 8900 mm (fixed-ended 70×1.2 mm columns), (ii) 3000, 4000 mm (fixed-ended 50×1.2 mm columns), (iii) 1000, 1500, 2000 mm (fixed-ended 50×2.6 mm columns) and (iv) 1820, 2520, 3640, 4200 mm (pin-ended 70×1.2 mm columns).

All the cross-section dimensions, lengths, yield stresses f_y and numerical (SFEA) ultimate stresses f_u are given in Table 3 (89 fixed-ended columns) and in Table 4 (28 pin-ended columns).

4. DSM Design Considerations

Regarding the existing design provisions for concentrically loaded equal-leg angle columns, the earlier AISI (1996) and NAS (AISI 2001) specifications prescribed ultimate strength estimates of the form

$$P_n = A_e \times f_n \quad , \quad (1)$$

where A_e is the angle effective cross-section area and f_n is the column global strength, given by

$$f_n = \begin{cases} f_y \left(0.658^{\lambda_c^2} \right) & \text{if } \lambda_c \leq 1.5 \\ f_y \left(\frac{0.877}{\lambda_c^2} \right) & \text{if } \lambda_c > 1.5 \end{cases} \quad \text{with} \quad \lambda_c = \sqrt{\frac{f_y}{f_{cre}}} \quad , \quad (2)$$

where f_y is the yield stress, f_{cre} is the critical global buckling stress and λ_c is the global slenderness. Since (i) f_n is based on the minimum between the flexural-torsional (major-axis) and flexural (minor-axis) buckling stresses, and (ii) A_e is based on the local (or torsional) buckling stress, Popovic *et al.* (2001) showed that the above procedure led to overly conservative P_n values, due to the fact that the torsional buckling stress comes into play twice (through f_n and A_e). In order to achieve more accurate (but still safe) ultimate strength predictions, these authors proposed a modification: to base (i) f_n on the flexural (minor-axis) buckling stress alone, and (ii) A_e on the local (torsional) buckling stress. Later, Young (2004) tested fixed-ended angle columns and showed that the modified AISI/NAS estimates were (i) still conservative for stocky columns and (ii) unsafe for slender columns. In order to obtain more accurate estimates, he proposed the use of a modified global strength curve, given by

$$f_{ne} = \begin{cases} f_y \left(0.5^{\lambda_c^2} \right) & \text{if } \lambda_c \leq 1.4 \\ f_y \left(\frac{0.5}{\lambda_c^2} \right) & \text{if } \lambda_c > 1.4 \end{cases} \quad \text{with} \quad \lambda_c = \sqrt{\frac{f_y}{f_{cre}}} \quad . \quad (3)$$

where f_{cre} is the minor-axis flexural buckling stress. The column ultimate strength is still determined on the basis of Eq. (1), but replacing f_n by f_{ne} . Rasmussen (2005) followed a different path to design slender pin-ended angle columns, arguing that the angle singly-symmetry called for the consideration of an additional moment due to the effective centroid shift. Quantifying this additional moment required (i)

Table 3: Fixed-ended column numerical ultimate stresses and their estimates according to the proposed DSM-based approach

Section	L (mm)	Buckling analysis		f_y (N/mm ²)	Numerical	DSM-F	Numerical- to-Predicted
		f_{cr1} (N/mm ²)	f_{cre} (N/mm ²)		f_u (N/mm ²)	f_{nle} (N/mm ²)	f_u/f_{nle}
70x1.2	532	27.5	5981	30	25.5	24.7	1.03
	980	24.8	1762		24.3	23.7	1.02
	1330	24.2	957		24.1	23.4	1.03
	1820	23.9	511		24.0	23.0	1.04
	2520	23.6	267		23.9	22.4	1.07
	3640	23.3	128		23.7	21.0	1.13
	4200	23.2	96		19.3	20.3	0.95
	5320	22.8	60		18.1	18.4	0.98
	7000	22.1	35		14.5	15.4	0.94
	8900	21.1	21		11.3	11.3	1.00
	532	27.5	5981	60	36.7	38.9	0.94
	980	24.8	1762		34.7	37.1	0.93
	1330	24.2	957		33.3	36.3	0.92
	1820	23.9	511		31.7	35.3	0.90
	2520	23.6	267		29.7	33.5	0.89
	3640	23.3	128		28.6	29.9	0.96
	4200	23.2	96		20.6	27.8	0.74
	5320	22.8	60		19.3	23.2	0.83
	7000	22.1	35		15.5	16.4	0.95
	8900	21.1	21		12.8	10.7	1.20
	532	27.5	5981	120	65.7	60.5	1.09
	980	24.8	1762		63.8	57.0	1.12
	1330	24.2	957		61.8	55.1	1.12
	1820	23.9	511		57.7	52.3	1.10
	2520	23.6	267		49.2	47.3	1.04
	3640	23.3	128		35.5	37.9	0.94
	4200	23.2	96		24.1	32.9	0.73
	5320	22.8	60		21.4	23.2	0.92
	7000	22.1	35		15.6	15.9	0.98
	8900	21.1	21		12.8	10.7	1.20
	532	27.5	5981	235	110	91.7	1.20
	980	24.8	1762		106	84.7	1.25
	1330	24.2	957		93.7	79.9	1.17
	1820	23.9	511		71.8	72.5	0.99
	2520	23.6	267		55.1	60.0	0.92
	3640	23.3	128		37.9	39.1	0.97
	4200	23.2	96		29.7	31.9	0.93
	5320	22.8	60		23.5	23.2	1.01
	7000	22.1	35		15.6	15.9	0.98
	8900	21.1	21		12.8	10.7	1.20
	532	27.5	5981	400	145	126.3	1.15
	980	24.8	1762		122	113.4	1.08
	1330	24.2	957		98	103.5	0.95
	1820	23.9	511		72	87.9	0.82

Section	L (mm)	f_{cr1} (N/mm ²)	f_{cre} (N/mm ²)	f_y (N/mm ²)	f_u (N/mm ²)	f_{nle} (N/mm ²)	f_u/f_{nle}		
	2520	23.6	267	400	55	64.0	0.86		
	3640	23.3	128		36	38.4	0.94		
	4200	23.2	96		30.3	31.9	0.95		
	5320	22.8	60		24.1	23.2	1.04		
	7000	22.1	35		15.6	15.9	0.98		
	8900	21.1	21		12.8	10.7	1.20		
	532	27.5	5981	500	163	144.1	1.13		
	980	24.8	1762		135	127.1	1.06		
	1330	24.2	957		105	113.6	0.92		
	1820	23.9	511		72	92.9	0.78		
	2520	23.6	267		55	62.5	0.88		
	3640	23.3	128		36	38.4	0.94		
	4200	23.2	96		30.3	31.9	0.95		
	5320	22.8	60		24.1	23.2	1.04		
	7000	22.1	35		15.6	15.9	0.98		
	8900	21.1	21		12.8	10.7	1.20		
	50×1.2	1500	46.3		383.8	120	58	63.9	0.91
		2000	45.6		215.9		56	57.0	0.98
2500		45	138.2	54	49.2		1.10		
3000		44.3	96.0	36.6	41.1		0.89		
4000		42.6	54.0	29.1	26.6		1.10		
1500		46.3	383.8	235	88	86.3	1.02		
2000		45.6	215.9		67	69.4	0.97		
2500		45	138.2		55	52.4	1.05		
3000		44.3	96.0		38	39.7	0.96		
4000		42.6	54.0		29.1	26.6	1.10		
1500		46.3	383.8	400	89	100.2	0.89		
2000		45.6	215.9		67	69.5	0.96		
2500		45	138.2		55	50.8	1.08		
3000		44.3	96.0		38.9	39.7	0.98		
4000		42.6	54.0		29.1	26.6	1.10		
1500		46.3	383.8	500	89	103.0	0.86		
2000		45.6	215.9		67	68.3	0.98		
2500		45	138.2		55	50.8	1.08		
3000		44.3	96.0		39	39.7	0.98		
4000		42.6	54.0		29.1	26.6	1.10		
50×2.6	1000	214.2	863.6	120	111	109.0	1.02		
	1500	205	383.8		100	96.6	1.03		
	2000	194.6	215.9		87.8	81.6	1.08		
	1000	214.2	863.6	235	202	170.7	1.18		
	1500	205	383.8		176	143.5	1.23		
	2000	194.6	215.9		128	110.5	1.16		
	1000	214.2	863.6	400	230	222.8	1.03		
	1500	205	383.8		192	168.1	1.14		
	2000	194.6	215.9		132	110.7	1.19		
						Mean	1.01		
						Sd. Dev.	0.11		

Table 4: Pin-ended column numerical ultimate stresses and their estimates according to the two proposed DSM-based approaches

Section	L (mm)	Buckling analysis			Numerical	DSM-F	Numerical- to-Predicted	DSM-P	Numerical- to-Predicted	
		f_{cr1} (N/mm ²)	f_{cre} (N/mm ²)	f_y (N/mm ²)	f_u (N/mm ²)	f_{nle} (N/mm ²)	f_u/f_{nle}	f_{nle} (N/mm ²)	f_u/f_{nle}	
70x1.2	532	27.4	1496	30	24.6	24.5	1.00	21.1	1.17	
	980	24.8	441	30	23.6	23.2	1.02	19.4	1.22	
	1330	24.2	234	30	23.3	22.4	1.04	18.9	1.23	
	1820	23.9	128	30	20.7	21.2	0.98	18.3	1.13	
	2520	23.7	67	30	18.7	19.1	0.98	17.3	1.08	
	3640	23.4	32	30	15.1	15.1	1.00	14.6	1.03	
	4200	23.2	24	30	13.2	12.6	1.05	12.6	1.05	
	532	27.4	1496	60	27.1	38.4	0.71	24.2	1.12	
	980	24.8	441	60	24.6	35.4	0.69	21.9	1.12	
	1330	24.2	234	60	23.9	33.3	0.72	21.3	1.12	
	1820	23.9	128	60	21	30.1	0.70	20.6	1.02	
	2520	23.7	67	60	18.8	24.7	0.76	19.3	0.97	
	3640	23.4	32	60	15.3	15.6	0.98	15.0	1.02	
	4200	23.2	24	60	13.4	12.0	1.12	12.0	1.12	
	532	27.4	1496	120	29.6	58.9	0.50	25.8	1.15	
	980	24.8	441	120	26.9	52.1	0.52	23.2	1.16	
	1330	24.2	234	120	25.5	46.5	0.55	22.5	1.13	
	1820	23.9	128	120	21	38.2	0.55	21.6	0.97	
	2520	23.7	67	120	18.8	25.8	0.73	19.6	0.96	
	3640	23.4	32	120	15.3	15.3	1.00	14.8	1.03	
	4200	23.2	24	120	13.4	12.0	1.12	12.0	1.12	
	532	27.4	1496	235	39.2	87.1	0.45	26.6	1.48	
	980	24.8	441	235	30.3	71.1	0.43	23.8	1.27	
	1330	24.2	234	235	25.7	57.4	0.45	23.0	1.12	
	1820	23.9	128	235	21	39.5	0.53	21.7	0.97	
	2520	23.7	67	235	18.8	25.3	0.74	19.5	0.97	
	3640	23.4	32	235	15.3	15.3	1.00	14.8	1.03	
	4200	23.2	24	235	13.4	12.0	1.12	12.0	1.12	
	Mean							0.80	Mean	1.10
	Sd. Dev.							0.24	Sd. Dev.	0.11

calculating an angle cross-section “effective modulus” for minor-axis bending and (ii) using an N-M interaction formula – but the extra work paid off, since this approach was shown to yield more accurate ultimate strength estimates than its predecessors.

In the last decade, the Direct Strength Method (DSM) emerged as a simple and reliable approach to design cold-formed steel members, and has already been included in the most recent North American (2007) and Australian/New Zealand (2005) cold-formed steel specifications. The DSM approach is based on the Winter-type local strength curve (Schafer 2008)

$$f_{nl} = \begin{cases} f_y & \text{if } \lambda_l \leq 0.776 \\ f_y \left(\frac{f_{cr1}}{f_y} \right)^{0.4} \left[1 - 0.15 \left(\frac{f_{cr1}}{f_y} \right)^{0.4} \right] & \text{if } \lambda_l > 0.776 \end{cases} \quad \text{with} \quad \lambda_l = \sqrt{\frac{f_y}{f_{cr1}}} \quad , \quad (4)$$

where f_{crl} and f_{nl} are the local buckling stress and strength. However, and since the column local and global failures often interact, the current DSM combines Eq. (4), for local failure, with Eq. (2), for global failure – f_y is replaced by f_{ne} in Eq. (4). The current DSM curve for local/global interactive collapse then reads

$$f_{nle} = \begin{cases} f_{ne} & \text{if } \lambda_{le} \leq 0.776 \\ f_{ne} \left(\frac{f_{crl}}{f_{ne}} \right)^{0.4} \left[1 - 0.15 \left(\frac{f_{crl}}{f_{ne}} \right)^{0.4} \right] & \text{if } \lambda_{le} > 0.776 \end{cases} \quad \text{with} \quad \lambda_{le} = \sqrt{\frac{f_{ne}}{f_{crl}}}, \quad (5)$$

where f_{nle} is the local/global interactive strength, f_{ne} is the global strength, obtained from Eq. (2), and f_{crl} is the critical local buckling stress. The column ultimate load is given by

$$P_n = A \times f_{nle}, \quad (6)$$

where A is the gross cross-section area. In Eq. (1), the local and global buckling effects are dealt with separately by means of the effective area A_e and global buckling strength f_n , respectively. Conversely, they are handled simultaneously in Eq. (6), through the local/global interactive strength f_{nle} .

Several cross-section geometries (*e.g.*, lipped channels, Z-sections, rack-sections or hat-sections) are currently pre-qualified for the application of the DSM. Despite their extreme geometrical simplicity, angle sections did not yet achieved such status, *i.e.*, they are not pre-qualified for the application of the current DSM design curves. Nevertheless, Rasmussen (2006) and Chodraui *et al.* (2006) proposed distinct DSM-based approaches for the design of concentrically loaded angle columns. While the former incorporates explicitly the eccentricity due to the effective centroid shift, which amounts to treating the columns as beam-columns, the latter ignores the above eccentricity, exploring instead different relations between the local (flexural-torsional) and global (minor-axis flexural) buckling stresses. At this stage, it is worth mentioning that Dinis *et al.* (2011) have shown that the straightforward use of current DSM design curves (combination of Eqs. (2) and (5)) leads to a significant number of poor ultimate strength predictions, which is just an obvious and natural cause/consequence of the fact that angle columns are not pre-qualified for the DSM application.

While in Eqs. (2)-(3) it is mandatory to calculate the minor-axis flexural buckling stress f_{cre} , Eqs. (4)-(5) require the knowledge of the local buckling stress f_{crl} , replaced herein (equal-leg angle columns) by the flexural-torsional buckling stress⁶. In this work, these two buckling stresses were determined by means of the code GBTUL (Bebiano *et al.* 2008a,b), taking into account the column (i) actual end support conditions (fixed or pinned end sections) and (ii) experimentally measured cross-section dimensions and steel properties – the f_{crl} and f_{cre} values are given in (i) Tables 1 and 2 (experimental ultimate strengths) and (ii) Tables 3 and 4 (numerical ultimate strengths). It is worth mentioning that the signature curves $f_{crl}(L)$ and $f_{cre}(L)$ shown in Figures 9 and 10 were obtained by means of two separate GBT analyses (see Figure 1(b)): (i) ones including modes **2** (major-axis bending), **4** (torsion) and **6** (anti-symmetric local), to

⁶ Note that the local buckling stress f_{crl} must be equated to the flexural-torsional buckling stress. Due to the presence of the flexural component, the “local” buckling of equal-leg angles cannot be viewed as the usual local buckling of other sections. Because the corner flexural displacements have been shown to play a key role in the column post-critical strength, the mechanics of “local” buckling should not be equated solely to torsional buckling and the angle column behavior cannot be viewed as the “sum” of two pinned-free long plates. Thus, the flexural component of the buckling mode should not be omitted, even if its contribution does not alter the design strength predictions significantly.

obtain the $f_{cr}(L)$ curve, and (ii) the others including only mode **3** (minor-axis bending), to obtain the $f_{cre}(L)$ curve. The $f_{cr}(L)$ curve corresponds to clamped support conditions for modes **2**, **4** and **6**, both in the pin-ended and fixed-ended columns. The $f_{cre}(L)$ curve was obtained considering clamped or pinned support conditions for mode **3**, respectively for the fixed-ended and pin-ended columns.

Figures 9(a)-(b) and 10(a)-(b) show the signature curves $f_{cr}(L)$ of (i) the fixed-ended columns tested by Popovic *et al.* (1999) (Fig. 9(a)) and Young (2004) (Fig. 9(b)), and (ii) the pin-ended columns tested by Popovic *et al.* (1999) (Fig. 10(a)), Chodraui *et al.* (2006) and Maia *et al.* (2008) (Fig. 10(b))⁷. The dashed and thinner solid curves correspond to the flexural-torsional buckling stress f_{cr} and the thicker solid curve corresponds to the minor-axis flexural buckling stress f_{cre} ⁸ – the column critical stresses correspond to the lower of f_{cr} and f_{cre} . The white and black circles, located respectively on the $f_{cr}(L)$ and $f_{cre}(L)$ curves, identify the lengths of the columns tested by the various researchers.

Concerning the fixed-ended columns (Figs. 9(a)-(b)), it is clear that all the columns tested by Young are located far away (to the left) from the intersection between the $f_{cr}(L)$ and $f_{cre}(L)$ curves, which means that f_{cre} is always much higher than f_{cr} – the lowest f_{cre}/f_{cr} ratio is equal to 2.7, corresponding to the longest column ($L=3500\text{mm}$) with the stockiest cross-section ($70\times 1.9\text{mm}$). Conversely, most of the fixed-ended columns tested by Popovic *et al.* have lengths placing them on the right side of the $f_{cr}(L)$ curve horizontal plateaus, *i.e.*, the near their intersection with $f_{cre}(L)$, which means f_{cre}/f_{cr} values close to 1.0 – the few exceptions concern some $50\times 2.5\text{mm}$ column lengths, located on the left side of the $f_{cr}(L)$ curve horizontal plateau. Moreover, in some of these columns the minor-axis flexural buckling mode becomes “critical” (*i.e.*, $f_{cre}/f_{cr} < 1.0$).

Concerning the pin-ended columns (Figs. 10(a)-(b)), most of their lengths place them on the right side of the $f_{cr}(L)$ curve horizontal plateaus – the exceptions are the shortest (i) $50\times 2.5\text{mm}$ columns tested by Popovic *et al.* and (ii) columns tested by Chodraui *et al.*, which are located on the left side of the $f_{cr}(L)$ curve horizontal plateaus.

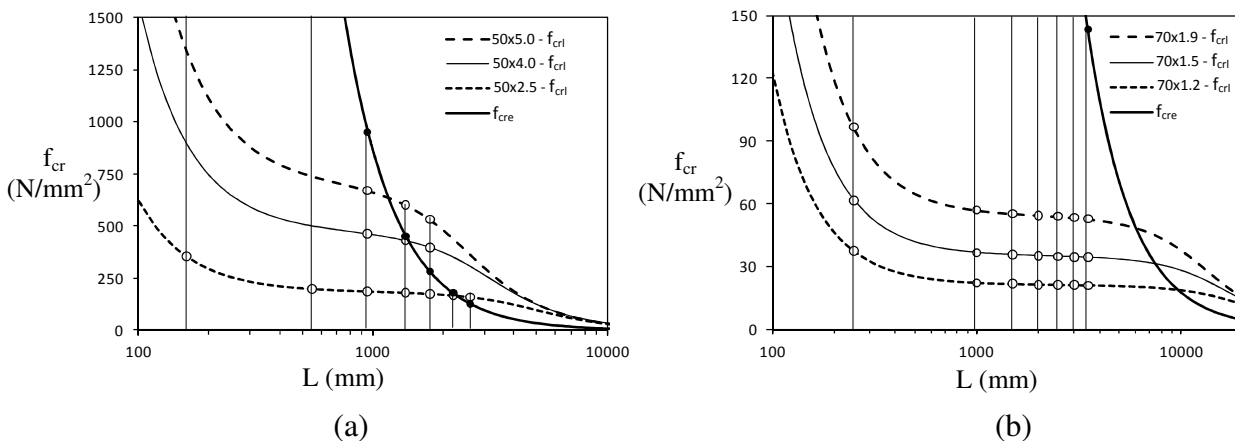


Figure 9: Variation of f_{cr} with L for the fixed-ended columns tested by (a) Popovic *et al.* (1999) and (b) Young (2004)

⁷ None of these figures concerns the fixed-ended columns tested by Mesacasa Jr. (2011).

⁸ One flexural-torsional curve per cross-section geometry and a common minor-axis flexural curve for all cross-sections sharing the same mid-line dimensions – this amounts to neglecting the contributions of the wall “own inertias” to the cross-section minor moment of inertia.

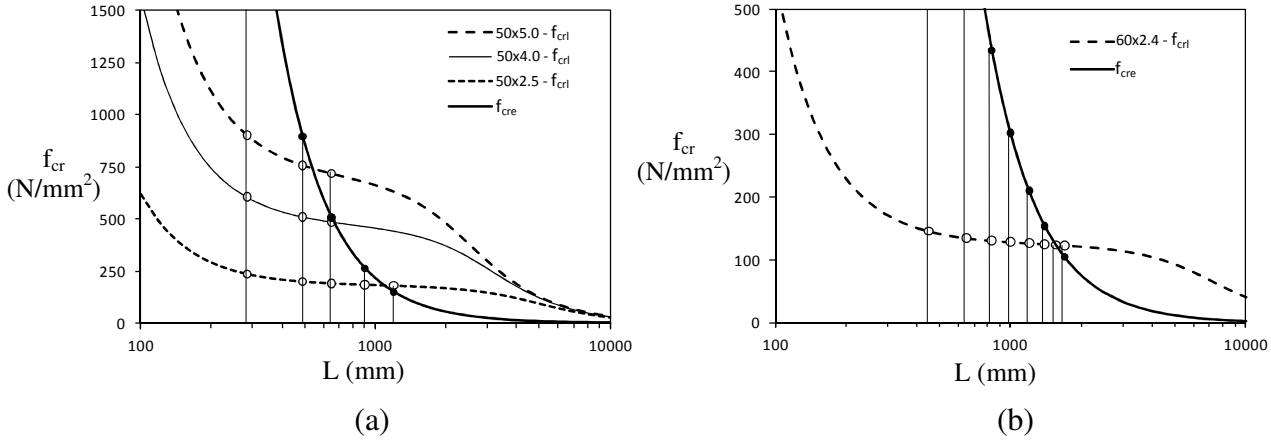


Figure 10: Variation of f_{cr} with L for the pin-ended columns tested by (a) Popovic *et al.* (1999) and (b) Chodraui *et al.* (2006) and Maia *et al.* (2008)

It will be shown later that, both in fixed-ended and pin-ended columns, the ultimate strength is strongly affected by the “location” of the column length, *i.e.*, the “closeness” between the f_{cr} and f_{cre} values. As mentioned previously, the shorter columns, located on the left side of the plateaus, have clearly stable post-critical behaviors, since they exhibit very small corner displacements. Conversely, the longer columns, located on the right side of the plateaus possess a minute/negligible post-buckling strength, since they exhibit significant corner displacements, stemming predominantly from minor-axis flexure (even with $f_{cre}/f_{cr} > 1.0$, *i.e.*, minor-axis flexural buckling is “non-critical”).

After having determined the f_{cr} and f_{cre} values of all the columns, given in Tables 1-4, it becomes possible to calculate their minor-axis flexural and flexural-torsional slenderness values, given by $\lambda_c = \sqrt{f_y / f_{cre}}$ and $\lambda_l = \sqrt{f_y / f_{cr}}$. Figures 11(a)-(b) (fixed-ended columns) and 12(a)-(b) (pin-ended columns) show the variation of the ultimate-to-yield stress ratio values (f_u/f_y), obtained from the experimental (white circles) and numerical (black circles) results, with both λ_c (Figs. 11(a) and 12(a)) and λ_l (Figs. 11(b) and 12(b)) – note that the thin solid line in Fig. 12(b) identifies a strength curve proposed by Rasmussen (2005), addressed below. The solid lines in these figures correspond to the global (f_{ne}/f_y – Eq. (2)) and local (f_{nl}/f_y – Eq. (4)) DSM design curves. The observation of these figures prompts the following comments:

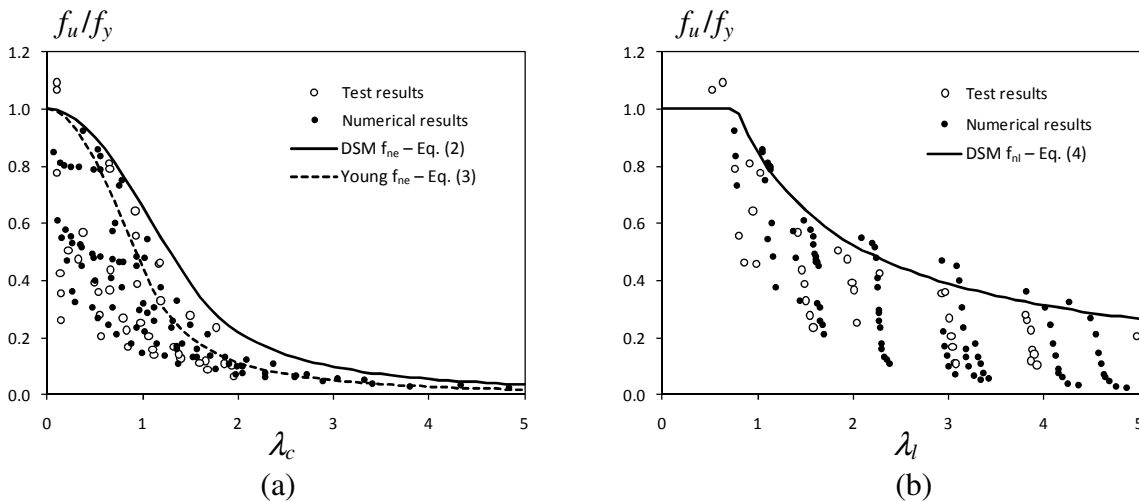


Figure 11: Fixed-ended columns: variation of f_u/f_y with (a) λ_c and (b) λ_l

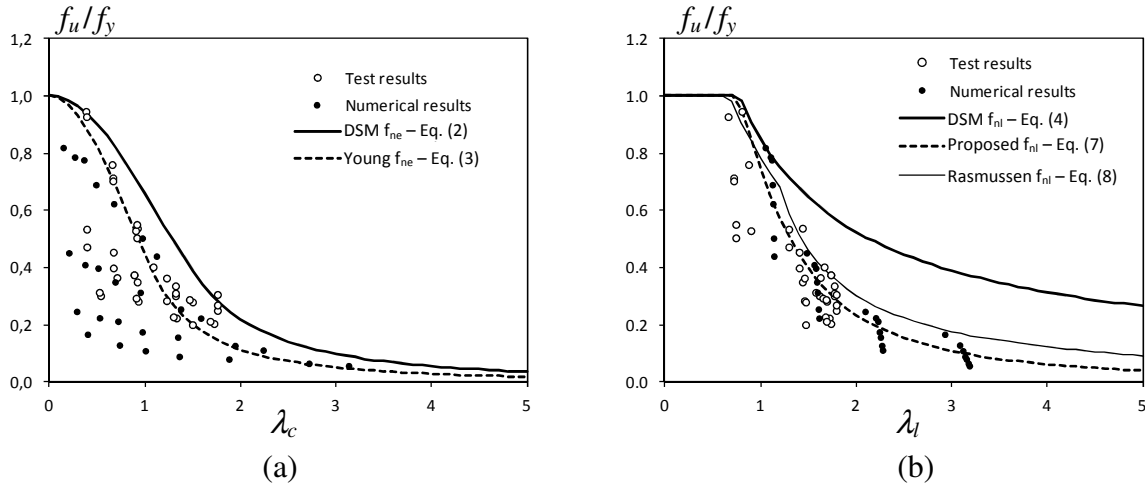


Figure 12: Pin-ended columns: variation of f_u/f_y with (a) λ_c and (b) λ_l

- (i) In each figure, the clouds of white and black circles share nearly the same location, showing that the experimental and numerical ultimate strengths exhibit similar overall tendencies.
- (ii) Regardless of the global or local slenderness range, the vast majority of f_u/f_y values fall well below the DSM curves, thus showing/confirming that the DSM “pure” global and local strength curves consistently overestimate the angle column ultimate strengths by fairly large margins.
- (iii) The f_u/f_y values are widely spread for low-to-moderate global slenderness values λ_c , but become less scattered for higher λ_c values. Figs. 11(a) and 12(a) also show the global strength curve (Eq. (3) – dashed line) proposed by Young (2004). It is clear that this curve follows the tendency of the f_u/f_y values much more closely than the current DSM global strength curve (Eq. (2) – solid line), particularly for moderate-to-high global slenderness values λ_c .
- (iv) Due to the small variation (drop) of f_{cr1} with L within the $f_{cr1}(L)$ curve horizontal plateau, the f_u/f_y values concerning the columns with the same yield stress are clearly “grouped together” in Figs. 11(b) and 12(b). As f_y increases, the corresponding group is associated with a higher local slenderness λ_l and a lower strength (*i.e.*, moves down and to the right) – within each group, the slenderness increases with the length L .
- (v) Within each group, the variation of f_u/f_y with λ_l is markedly different for the fixed-ended and pin-ended columns. While the fixed-ended columns (Fig. 11(b)) exhibit a high “vertical dispersion”, thus implying a very significant variation of f_u/f_y with L (even if f_{cr1} remains practically unaltered), those concerning the pin-ended columns (Fig. 12(b)) are rather “packed together” and located considerably below the DSM local curve (Eq. (4)). This behavioral difference is mainly due to the influence of the effective centroid shift, which was shown to be much more relevant in pin-ended columns than in their fixed-ended counterparts. This effect was considered in the rational design methodology developed by Rasmussen (2005, 2006) and based on the “beam-column concept”: the additional moment, due to the compressive force action on the eccentricity due to the effective centroid shift, was taken into account by using a beam-column interaction equation.
- (vi) In spite of the quite pronounced qualitative and quantitative differences detected in the elastic post-buckling behaviors of the pin-ended columns (see the results presented earlier), the differences between their ultimate strengths are only moderate. Note that the f_u/f_y values corresponding to the pin-ended columns, displayed in Fig. 12(b), are only slightly grouped together and show a tendency to vary with the local slenderness λ_l . Thus, it seems possible (and may be advantageous) to fit a

new strength curve for the design against “local” (flexural-torsional, in reality) failure of pin-ended angle columns, which is given by

$$f_{nl} = \begin{cases} f_y & \text{if } \lambda_l \leq 0.71 \\ f_y \left(\frac{f_{crit}}{f_y} \right) \left[1 - 0.25 \left(\frac{f_{crit}}{f_y} \right) \right] & \text{if } \lambda_l > 0.71 \end{cases} \quad \text{with} \quad \lambda_l = \sqrt{\frac{f_y}{f_{crit}}} \quad . \quad (7)$$

Figure 12(b) depicts this curve and it is clear that it follows fairly well the trend of the f_u/f_y values. Moreover, since the influence of the effective centroid shift is directly taken into account, it should lead to an efficient design procedure for pin-ended angle columns without the need to resort to the beam-column concept. It should also be emphasized that this curve falls well below the current DSM local strength curve (applicable to columns with various pre-qualified cross-section shapes). This fact just shows that the interaction between *flexural-torsional* buckling and minor-axis flexural buckling in pin-ended angle columns is much more severe than the interaction between *local* and global (flexural or flexural-torsional) buckling in columns with other cross-section shapes. This stems from the extremely high sensitivity to the effective centroid shift, which was clearly demonstrated earlier in the paper and can be physically explained by the fact that both angle cross-section walls (legs) are *outstands* – in all the columns with cross-sections pre-qualified to the application of the DSM, local buckling is virtually always triggered by *internal* walls, which entails a considerably less severe interaction with global buckling.

- (vii) Conversely, the differences between the fixed-ended column ultimate strengths are rather sharp. Indeed, most of them are located in “almost vertical line segments”, thus meaning that columns sharing the same yield and critical stresses (but having different lengths) exhibit quite distinct f_u/f_y values. This somewhat “paradoxical” behavior appears to indicate that the local slenderness λ_l does not provide an adequate “measure” of the column ultimate strength. Recalling that most of these columns buckle in flexural-torsional modes “almost akin” to a local mode (see Fig. 1(c) – the word “almost” stems from the presence of corner flexural displacements), it seems fair to say that, within the $f_{crit}(L)$ curve horizontal plateau, the fixed-ended column ultimate strength nature “travels” from “local” to “global” as the length increases – an efficient design procedure for these columns must take this fact into account.
- (viii) The strength curve proposed by Rasmussen (2005) for pin-ended columns (solid thin line in Fig. 12(b)), which is given by

$$f_{nl} = \rho \cdot \beta \cdot f_y \quad (8)$$

$$\rho = \frac{A_e}{A} = \begin{cases} 1 & \text{if } \lambda_l \leq 0.673 \\ \frac{\lambda_l - 0.22}{\lambda_l^2} & \text{if } \lambda_l > 0.673 \end{cases} \quad \text{and} \quad \beta = \begin{cases} 1 & \text{if } \lambda_l \leq 1.22 \\ \frac{0.68}{(\lambda_l - 1)^{0.25}} & \text{if } \lambda_l > 1.22 \end{cases}$$

and takes into account (viii₁) the bending due to the effective centroid shift, through parameter β , and (ii) local (torsional) buckling, through the effective area reduction factor ρ . Although this curve also provides fairly accurate ultimate strength predictions, it is clear that it leads to slightly higher and less accurate ultimate strength predictions than the curve proposed in Eq. (7).

One last word to mention that the DSM distortional buckling curve is not considered in this work because this buckling mode does not occur in plain angles – the interested reader is referred to the work of Silvestre & Camotim (2010) for a mechanical definition of distortional buckling.

4.1 Proposal of a DSM-Based Design Approach

In order to enable the application of the “DSM philosophy” to the design of fixed-ended and pin-ended equal angle columns, the following DSM-based approach is proposed herein:

- (i) To adopt different procedures/design curves to estimate the ultimate strength of fixed-ended and pin-ended columns – they are designated as “DSM-F” and “DSM-P”, respectively.
- (ii) The DSM-F procedure combines (ii₁) Eq. (3), which is the global strength curve proposed by Young (2004), with (ii₂) Eq. (5), which is the current DSM design curve for local/global interactive failure. Although this procedure was developed specifically for fixed-ended columns, its application to pin-ended columns is also assessed.
- (iii) The DSM-P procedure combines Eq. (3), as before, with a proposed/new DSM curve for “local”/global interactive failure, defined by (see Fig. 12(b))

$$f_{nle} = \begin{cases} f_{ne} & \text{if } \lambda_{le} \leq 0.71 \\ f_{ne} \left(\frac{f_{crl}}{f_{ne}} \right) \left[1 - 0.25 \left(\frac{f_{crl}}{f_{ne}} \right) \right] & \text{if } \lambda_{le} > 0.71 \end{cases} \quad \text{with} \quad \lambda_{le} = \sqrt{\frac{f_{ne}}{f_{crl}}}, \quad (9)$$

which only differs from Eq. (5) in the fact that the yield stress f_y is replaced by the global strength f_{ne} . It is worth emphasizing again that this procedure is applied solely to pin-ended columns, which constitute the specific target of its development.

Attention is now turned to assessing the performance of the proposed DSM-based approach, *i.e.*, the DSM-F and DSM-P procedures. The corresponding column ultimate strength predictions (f_{nle} values) are included in Tables 1-4. The ultimate-to-predicted strength ratios (f_u/f_{nle}) are also given, where the ultimate strengths f_u correspond to the test values (Tables 1-2) and numerical values (Tables 3-4). In addition, Table 1 also gives the test-to-predicted ratio f_u/f_n values provided by the application of the methodology developed by Young (2004), which combines Eqs. (1) and (3), to the set of fixed-ended columns tested by Popovic *et al.* (1999) and Young (2004). On the other hand, Table 2 also presents the test-to-predicted ratios f_u/f_n obtained by Rasmussen (2006), with his beam-column methodology, for the pin-ended columns tested by Wilhoite *et al.* (1984) and Popovic *et al.* (1999). The close observation of the ultimate strength estimates presented in Tables 1-4 leads to the following remarks:

- (i) The DSM-F procedure leads to fairly accurate estimates of the fixed-ended column experimental ultimate strength values (see Table 1) – f_u/f_{nle} average and standard deviation of 0.98 and 0.14. The methodology developed by Young (2004) leads to considerably more conservative results – f_u/f_n average and standard deviation of 1.15 and 0.18.
- (ii) The DSM-F procedure also provides fairly accurate predictions of the fixed-ended column numerical ultimate strengths (see Table 3) – f_u/f_{nle} average and standard deviation of 1.01 and 0.11.
- (iii) Not surprisingly, the DSM-F procedure leads to accurate (in average) but widely scattered estimates of the pin-ended column experimental ultimate strengths (see Table 2) – f_u/f_{nle} average and standard deviation of 1.01 and 0.29. However, 16 (out of 37) predictions have errors higher than 20% (both safe and unsafe). This is due to the lack of proper accounting for the effective centroid shift effect – the DSM-F procedure adopts the current DSM strength curve for local/global interactive failure

(Eq. (5)). Conversely, the DSM-P procedure leads to reasonably accurate and safe (but fairly scattered) estimates of the pin-ended column experimental ultimate strengths – f_u/f_{nle} average and standard deviation of 1.13 and 0.25. The design approach developed by Rasmussen (2006) yields more conservative and slightly less scattered ultimate strength predictions – f_u/f_n average and standard deviation of 1.26 and 0.21 (note that the lower scatter is also related with the smaller number of results involved).

- (iv) The DSM-F procedure also predicts rather poorly the pin-ended column numerical ultimate strengths (see Table 4), which are mostly largely overestimated – f_u/f_{nle} average and standard deviation of 0.80 and 0.24. As for the estimates provided by the DSM-P procedure, they are slightly conservative and exhibit a fairly low scatter – f_u/f_{nle} average and standard deviation of 1.10 and 0.11.
- (v) The ultimate-to-predicted (ultimate means test or numerical) stress ratios f_u/f_{nle} can be viewed and compared in Figs. 13(a) (fixed-ended columns) and 13(b) (pin-ended columns) – the white and black circles stand again for the experimental (test) and numerical results. With the exception of four less accurate pin-ended column ultimate strength estimates (white circles in Fig. 13(b) – 4 underestimations concerning eccentrically loaded columns tested by Wilhoite *et al.*), all the pin-ended and fixed-ended column f_u/f_{nle} values exhibit an acceptable scatter and vary randomly around 1.01 (fixed-ended columns) and 1.12 (pin-ended columns).
- (vi) While the fixed-ended column f_u/f_{nle} values are spread along a fairly wide local/global slenderness range, their pin-ended column counterparts are mostly “accumulated” in a limited local/global slenderness range ($0.5 < \lambda_{le} < 1.5$) – only numerical f_u/f_{nle} values fall outside of this range. In order to properly assess the accuracy of the DSM-P procedure in the full λ_{le} range, it is necessary to perform experimental tests on pin-ended columns with high local/global slenderness values ($\lambda_{le} > 1.5$). In this respect, it is worth mentioning that most of the (few) numerical ultimate strengths associated with high λ_{le} values are underestimated by the DSM-P procedure – this underestimation is larger for the two columns exhibiting λ_{le} values higher than 2.5.

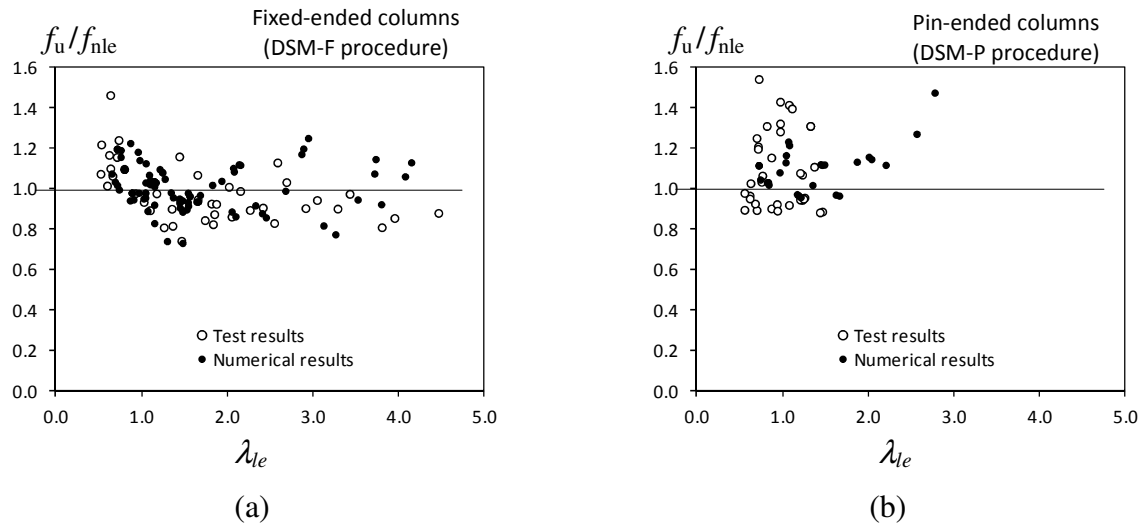


Figure 13: Variation of f_{nle}/f_u with λ_{le} for the (a) DSM-F (fixed-ended columns) (b) and DSM-P (pin-ended columns) procedures

Now, the determination of the LRFD (Load and Resistance Factor Design) resistance factor ϕ for the proposed DSM-based approaches is briefly addressed. According to the most recent North American cold-formed steel specification (AISI 2007), the resistance factor ϕ can be calculated using the formula given in section F.1.1 of chapter F, which reads

$$\phi = C_\phi (M_m F_m P_m) e^{-\beta_0 \sqrt{V_M^2 + V_F^2 + C_P V_P^2 + V_Q^2}} \quad \text{with} \quad C_P = \left(1 + \frac{1}{n}\right) \frac{m}{m-2}, \quad (10)$$

where (i) C_ϕ is a calibration coefficient ($C_\phi=1.52$ for LRFD), (ii) $M_m=1.0$ and $F_m=1.00$ are the mean values of the material and fabrication factor, respectively, (iii) β_0 is the target reliability index ($\beta_0=2.5$ for structural members in LRFD), (iv) $V_M=0.10$, $V_F=0.05$ and $V_Q=0.21$ are the coefficients of variation of the material factor, fabrication factor and load effect, respectively, and (v) C_P is a correction factor that depends on the number of tests (n) and degrees of freedom ($m=n-1$). In order to evaluate the resistance factor ϕ for each DSM-based procedure (DSM-F and DSM-P), it is necessary to calculate P_m and V_P , which are the mean and standard deviation values of the “exact”-to-predicted stress ratios f_u/f_{ule} – “exact” means either test f_u values, numerical f_u values or both test and numerical f_u values.

Table 5 shows the n , C_P , P_m , V_P and ϕ values obtained for the column ultimate strength estimates provided by the DSM-F (fixed-ended columns) and DSM-P (pin-ended columns) procedures using the test, numerical and overall (test plus numerical) data. The resistance factor values associated with each of the two proposed DSM-based procedures are (i) $\phi=0.81$ (fixed-ended columns) and $\phi=0.78$ (pin-ended columns), for the experimental data, and (ii) $\phi=0.89$ (fixed-ended columns) and $\phi=0.95$ (pin-ended columns), for the numerical data. When all the experimental and numerical data are considered together, the overall application of the DSM-F and DSM-P procedures leads to $\phi=0.87$ and $\phi=0.85$, values practically coincident with that recommended by the NAS (2007) – $\phi=0.85$. Therefore it may be readily concluded that the value $\phi=0.85$, which is employed when applying the current DSM, can also be safely adopted with the proposed DSM-F and DSM-P procedures. Additionally, the DSM-F approach was also tested for the pin-ended columns – recall that it uses Eqs. (3) and (5) and differs from the current DSM in the fact the global strength curve is replaced by the one proposed by Young (2004). The resistance factor values obtained are (see Table 5) $\phi=0.65$ (experimental), $\phi=0.56$ (numerical) and $\phi=0.60$ (experimental and numerical), well below the value recommended by the NAS (2007) – $\phi=0.85$. Therefore, the DSM-F approach can be adopted for pin-ended plain angle columns if $\phi=0.60$ is adopted (an even lower value would be required to enable the application of the current DSM), which lowers significantly the strength of any column due to the high scatter of the DSM-F predictions. The authors rather prefer the use of a new “local” buckling curve (*i.e.*, the DSM-P approach), leading to less scattered predictions, together with the recommended resistance factor $\phi=0.85$ – it is a more rational approach, reflecting the different mechanics of the pin-ended and fixed-ended plain angle behaviors.

Table 5: LRFD resistance factors ϕ calculated according to AISI (2007) – DSM-F and DSM-P procedures

	Fixed-Ended Columns			Pin-Ended Columns					
	DSM-F			DSM-F			DSM-P		
	Test	Num.	Test+Num.	Test	Num.	Test+Num.	Test	Num.	Test+Num.
n	41	89	130	37	28	65	37	28	65
C_P	1.078	1.035	1.024	1.087	1.119	1.048	1.087	1.119	1.048
P_m	0.980	1.023	1.010	1.007	0.800	0.918	1.133	1.103	1.120
V_P	0.145	0.105	0.120	0.288	0.237	0.285	0.245	0.111	0.198
ϕ	0.81	0.89	0.87	0.65	0.56	0.60	0.79	0.95	0.86

Finally, it is worth mentioning that Ganesan & Moen (2010, 2012) recently investigated whether the LRFD strength reduction factor for DSM design of cold-formed steel compression members can be increased above its current value of $\phi=0.85$, since this specific value was established about twenty years ago (AISI 1991), on the basis of 264 column tests. They considered a much larger set of concentrically

loaded column tests, namely 675 tests involving columns with plain channels, lipped channels, angles, Z-sections and hat-sections. In the particular case of concentrically loaded (*i.e.*, without the eccentricity $L/1000$) angle columns, Ganesan & Moen (2010) found that the current DSM resistance factor, based on 75 test results (50 and 25 for plain and lipped angles, respectively) is $\phi=0.71$. They argued that this very low value is due to the high coefficient of variation of test-to-predicted ratios for angle columns and concluded that “...*fundamental research on the mechanics of angle compression members is needed to improve existing design methods... The low values for the resistance factor for angle columns indicate that the fundamental behavior of angle section columns is yet to be completely understood and there is a need for more research in the future*”. The work reported in this paper showed that the proposed DSM-based approach is accurate and, above all, is also mechanically sound because (i) it separates the provisions for fixed-ended and pin-ended columns, due the qualitative and quantitative differences involving the effective centroid shift responsible for the interaction between flexural-torsional (“local”) and (minor-axis) flexural buckling, and (ii) it incorporates a recently developed (for fixed-ended columns only) global strength curve – this curve, which can be applied to both pin-ended and fixed-ended columns, is able to capture the strong influence of minor-axis flexural buckling (either critical or non-critical) on the column post-buckling behavior and strength. The fact that these relevant features are not contemplated in the current DSM is at the root of the inadequacy (Dinis *et al.* 2012) and very low load resistance factor (Ganesan & Moen 2010, 2012) associated with its application to equal-leg angle columns⁹.

It is still worth mentioning that the angle column problem addressed in this work is the simplest one: concentrically loaded plain equal-leg angle columns. Yet, the ultimate strength estimates provided by the current design methods (Main Specification and DSM) are not as good as those obtained for more complex sections, such as plain or lipped channels. The consideration of other relevant aspects, like load eccentricities, leg asymmetries or stiffened legs, only “hides” the pure, but rather singular, behavior of concentrically loaded plain equal-leg angle columns, which deserves to be investigated on its own. It is expected that the above effects can be successfully handled by a DSM approach similar to the one proposed in this work within specified limits, provided that the buckling loads involved are evaluated rigorously and account for all the relevant effects – the DSM pre-qualification procedure will be very helpful in the specification of those limits.

5. Conclusion

After summarizing recent findings concerning the buckling, post-buckling and ultimate strength behaviors of fixed-ended and pin-ended short-to-intermediate equal-leg angle columns, the paper addressed their design by means of a DSM-based approach. Since short-to-intermediate angle columns buckle in flexural-torsional modes “almost akin” to the local buckling modes exhibited by columns with other cross-section shapes, the first step consisted of adopting the “DSM concept” of local/global interactive failure. The curve proposed by Young (2004), in the context of fixed-ended columns, was adopted to estimate the column global strength, as it was found to provide more accurate fixed-ended and pin-ended column ultimate strength estimates than the current DSM curve.

The recent disclosure of distinct mechanical features in the post-buckling and ultimate strength behaviors of fixed-ended and pinned ended columns, showing that the latter are much more prone and sensitive to the occurrence of interaction between flexural-torsional (“local”) and global buckling modes, led to the

⁹ In particular, the local strength curve does not capture adequately the peculiar behavioral features associated with angle column flexural-torsional buckling.

adoption of a different “local” strength curve for each end support condition. While the current DSM local strength curve is retained for fixed-ended columns, a new strength curve was proposed for pin-ended columns. This last curve makes it possible to capture the effective centroid shift effects, much more relevant in pin-ended columns than in fixed-ended ones, quite accurately.

The DSM-based approach proposed for the design of fixed-ended and pin-ended equal-leg angle columns (i) adopts the “local”/global interactive failure concept and (ii) uses distinct procedures (“local” strength curves) for fixed-ended (DSM-F) and pin-ended (DSM-P) columns, thus reflecting more closely the actual angle column behavior. This design approach was shown (i) to provide fairly accurate ultimate strength predictions for a wide column slenderness range, while retaining the simplicity of the current DSM application, and (ii) to exhibit an overall performance that compares favorably with those displayed by the other methods available in the literature to design angle columns. Moreover, it was also shown that the LRFD resistance factor $\phi=0.85$, employed with the current DSM, can also be safely adopted when applying the proposed DSM approach.

Acknowledgements

The authors gratefully acknowledge (i) Mr. Enio Mesacasa Jr, for the work carried out during his stay in Lisbon and also for sharing some of his recent research results, and (ii) the financial support of FCT (Portuguese Foundation for Science and Technology), through the research project “Generalised Beam Theory (GBT) - Development, Application and Dissemination” (PTDC/ECM/108146/2008).

References

- AISI – American Iron and Steel Institute (1991). *LRFD Cold-Formed Steel Design Manual*, Washington DC.
- AISI – American Iron and Steel Institute (1996). *AISI Specification for the Design of Cold-Formed Steel Structural Members*, Washington DC.
- AISI – American Iron and Steel Institute (2001). *North American Specification for the Design of Cold-Formed Steel Structures (NAS)*, Washington DC.
- AISI – American Iron and Steel Institute (2007). *North American Specification for the Design of Cold-Formed Steel Structural Members (NAS)*, Washington DC.
- AS/NZS – Standards of Australia and Standards of New Zealand (2005). *Cold-Formed Steel Structures*, Sydney-Wellington.
- Bebiano R, Silvestre N, Camotim D (2008a). “GBTUL 1.0 β – Code for buckling and vibration analysis of thin-walled members”, freely available at <http://www.civil.ist.utl.pt/gbt>.
- Bebiano R, Silvestre N, Camotim D (2008b). “GBTUL – a code for the buckling analysis of cold-formed steel members”, *Proceedings of 19th International Specialty Conference on Recent Research and Developments in Cold-Formed Steel Design and Construction* (St. Louis, 14-15/10), R. LaBoube, W.-W. Yu (eds.), 61-79.
- Camotim D, Basaglia C, Bebiano R, Gonçalves R, Silvestre N (2010). “Latest developments in the GBT analysis of thin-walled steel structures”, *Proceedings of International Colloquium on Stability and Ductility of Steel Structures (SDSS’Rio 2010 – Rio de Janeiro, 8-10/9)*, E. Batista, P. Vellasco, L. Lima (eds.), 33-58.
- Chodraui GMB, Shifferaw Y, Malite M, Schafer BW (2006). “Cold-formed steel angles under axial compression”, *Proceedings of 18th International Specialty Conference on Cold-Formed Steel Structures* (Orlando, 26-27/10), R. LaBoube, W.W. Yu (eds.), 285-300.
- Dinis PB, Camotim D (2011). “Buckling, post-buckling and strength of equal-leg angle and cruciform columns: similarities and differences”, *Proceedings of 6th European Conference on Steel and Composite Structures (Eurosteel 2011 – Budapest, 31/8-2/9)*, L. Dunai, M. Iványi, K. Jármai, N. Kovács, L.G. Vigh (Eds.), ECCS (Brussels), 105-110 (vol. A).
- Dinis PB, Camotim D, Silvestre N (2010a). “On the local and global buckling behaviour of angle, T-section and cruciform thin-walled columns and beams”, *Thin-Walled Structures*, **48**(10-11), 786-797.
- Dinis PB, Camotim D, Silvestre N (2010b). “Post-buckling behaviour and strength of angle columns”, *Proceedings of International Colloquium on Stability and Ductility of Steel Structures (SDSS’10 Rio – Rio de Janeiro, 8-10/9)*, E. Batista, P. Vellasco, L. Lima (eds.), 1141-1150.

- Dinis PB, Camotim D, Silvestre N (2011). "On the design of steel angle columns", *Proceedings of 6th International Conference on Thin-Walled Structures (ICTWS 2011 – Timisoara, 5-7/9)*, D. Dubina, V. Ungureanu (eds.), 271-279.
- Dinis PB, Camotim D, Silvestre N (2012). "On the mechanics of angle column instability", *Thin-Walled Structures*, **52**, 80-89, March 2012.
- Ellobody E, Young B (2005). "Behavior of cold-formed steel plain angle columns", *Journal of Structural Engineering (ASCE)*, **131**(3), 469-478, 2005.
- Ganesan K, Moen CD (2010). *LRFD and LSD Resistance Factors for Cold-Formed Steel Compression Members*, Final Report to the AISI, CE/VPI-ST-10/04, Virginia Polytechnic Institute and State University, Blacksburg, VA 24061.
- Ganesan K, Moen CD (2012). "LRFD resistance factor for cold-formed steel compression members", *Journal of Constructional Steel Research*, in press (doi:10.1016/j.jcsr.2012.01.003)
- Gaylord EH, Wilhoite GM (1985). "Transmission towers: design of cold-formed angles", *Journal of Structural Engineering (ASCE)*, **111**(8), 1810-1825.
- Kitipornchai S, Chan SL (1987). "Nonlinear finite-element analysis of angle and tee beam-columns", *Journal of Structural Engineering (ASCE)*, **113**(4), 721-739.
- Maia WF (2008). *On the Stability of Cold-Formed Steel Angle Columns*, M.A.Sc. Thesis, School of Engineering at São Carlos, University of S. Paulo, Brazil. (Portuguese)
- Maia WF, Neto JM, Malite M. (2008). "Stability of cold-formed steel simple and lipped angles under compression", *Proceedings of 19th International Specialty Conference on Cold-Formed Steel Structures (St. Louis, 26-27/10)*, R. LaBoube, W.W. Yu (eds.), 111-125.
- Mesacasa Jr. EC (2011). *Structural Behavior and Design of Cold-Formed Steel Angle Columns*, Research Report, School of Engineering at São Carlos, University of S. Paulo, Brazil. (Portuguese)
- Popovic D, Hancock GJ, Rasmussen KJR (1999). "Axial compression tests of cold-formed angles", *Journal of Structural Engineering (ASCE)*, **125**(5), 515-523.
- Popovic D, Hancock GJ, Rasmussen KJR (2001). "Compression tests on cold-formed angles loaded parallel with a leg", *Journal of Structural Engineering (ASCE)*, **127**(6), 600-607.
- Rasmussen KJR (2005). "Design of angle columns with locally unstable legs", *Journal of Structural Engineering (ASCE)*, **131**(10), 1553-1560.
- Rasmussen KJR (2006). "Design of slender angle section beam-columns by the direct strength method", *Journal of Structural Engineering (ASCE)*, **132**(2), 204-211.
- Schafer BW (2008). "Review: the direct strength method of cold-formed steel member design", *Journal of Constructional Steel Research*, **64**(7-8), 766-778.
- Shi G, Liu Z, Chung KF (2009). "Numerical study on the local buckling of 420 MPa steel equal angle columns under axial compression", *Proceedings of 6th International Conference on Advances in Steel Structures (ICASS'09 – Hong Kong, 16-18/12)*, S.L. Chan (ed.), 387-394 (vol. I).
- Shifferaw Y, Schafer BW (2011). "Behavior and design of cold-formed steel lipped and plain angles", *USB Proceedings of SSRC Annual Stability Conference (Pittsburgh, 10-14/5)*.
- Simulia Inc. (2008). *Abaqus Standard* (vrs. 6.7-5).
- Silvestre N, Camotim D (2010). "On the mechanics of distortion in thin-walled open sections", *Thin-Walled Structures*, **48**(7), 469-481.
- Silvestre N, Dinis PB, Camotim D (2012). "Direct strength prediction of lipped channel columns experiencing local-plate/distortional interaction", *Journal of Structural Engineering (ASCE)*, accepted for publication.
- Stowell EZ (1951). "Compressive strength of flanges", *National Advisory Committee for Aeronautics (NACA)*, Report N° 1029.
- Wilhoite GM, Zandonini R, Zavelani A (1984). "Behaviour and strength of angles in compression: an experimental investigation", *Proceedings of ASCE Annual Convention and Structures Congress (San Francisco, 1-3/10)*.
- Young B (2004). "Tests and design of fixed-ended cold-formed steel plain angle columns", *Journal of Structural Engineering (ASCE)*, **130**(12), 1931-1940.
- Young B, Rasmussen KJR (1999). "Shift of effective centroid in channel columns", *Journal of Structural Engineering (ASCE)*, **125**(5), 524-531.